

Forschungszentrum Karlsruhe
Technik und Umwelt

Wissenschaftliche Berichte
FZKA 5972

**Measurement of the Onset of
MHD-turbulence Caused by a Step
in the Electrical Conductivity in
the Channel Walls of GALINKA II
and Comparisons with Theoretical
Models**

F. Debray

Institut für Angewandte Thermo- und Fluidodynamik

August 1997

FORSCHUNGSZENTRUM KARLSRUHE
Technik und Umwelt
Wissenschaftliche Berichte
FZKA 5972

**Measurement of the onset of MHD-turbulence caused
by a step in the electrical conductivity in the channel
walls of GALINKA II and comparisons with theoretical
models**

*François Debray**

Institut für Angewandte Thermo- und Fluidodynamik

*Permanent Address:
Laboratoire des Champs Magnetiques Intenses MPI-CNRS

Forschungszentrum Karlsruhe GmbH, Karlsruhe
1997

Als Manuskript gedruckt
Für diesen Bericht behalten wir uns alle Rechte vor
Forschungszentrum Karlsruhe GmbH
Postfach 3640, 76021 Karlsruhe
Mitglied der Hermann von Helmholtz-Gemeinschaft
Deutscher Forschungszentren (HGF)
ISSN 0947-8620

ABSTRACT

The onset of 2-dimensional MHD-turbulence on shear layers with steep velocity gradients has been investigated experimentally. By choosing a special distribution of the electrical conductivity of the walls it is possible to create initial velocity profiles which lose their stability and show time dependent vortex flow pattern once the parameters exceed critical limits. The experiments have been conducted in a "horse track" loop being installed in the dipole magnet of the MEKKA facility. The distribution of the electrical conductivity of the walls has been realized by a copper strip embedded in the electrically insulating walls. The experimental results of the stability limits as well as of the spectral power density agree very well with the results of a theoretical model. A 6x11 potential probe array has been developed serving as an instrument to obtain a direct image of the vortex structure.

KURZFASSUNG

Messungen zum Einsetzen der durch eine stufenförmig verteilte elektrische Leitfähigkeit in den Kanalwänden von GALINKA II verursachten MHD-Turbulenz und Vergleich mit theoretischen Modellen

Das Einsetzen der 2-dimensionalen MHD-Turbulenz von Scherschichten mit steilen Geschwindigkeitsgradienten wird untersucht. Durch die Wahl einer besonderen Verteilung der Leitfähigkeit der Wände ist es möglich, Geschwindigkeitsprofile zu erzeugen, welche ihre Stabilität verlieren und ein zeitabhängiges Wirbelmuster zeigen, sobald die Parameter kritische Werte übersteigen. Die Experimente werden in einem "Horse Track" Kreislauf durchgeführt, der in dem Dipolmagnet der MEKKA-Anlage eingebaut ist. Die Verteilung der elektrischen Leitfähigkeit der Wände wird durch einen Kupferstreifen erreicht, der in die elektrisch isolierten Wände eingebettet ist. Die experimentellen Ergebnisse für die Stabilitätsgrenze und auch für die spektrale Leistungsverteilung stimmen sehr gut mit den Ergebnissen eines theoretischen Modells überein. Eine Potentialsonde mit 6x11 Meßpunkten wurde entwickelt. Sie dient als Instrument zur Erzeugung von direkten Momentanaufnahmen der Wirbelstruktur.

CONTENTS

INTRODUCTION.....	1
I- EXPERIMENTAL DEVICE	2
I-1 General presentation.....	2
I-2 Aim of the measurements.....	3
I-3 The velocity measurements	4
I-3.1 Order of magnitude of the potential measurements.....	5
I-3.2 Amplification of the signal.....	7
I-4 Summary	9
II EXPERIMENTAL RESULTS	10
II-1 Dimensionless characteristic numbers.....	10
II-2 Comparison with the linear analysis	11
II-2.1 Threshold of instability	12
II-2.2 Calculation of the critical propagation velocity	14
II-2.3 Calculation of the critical wave number	14
II-2.4 Conclusion for the comparison between the results and the linear analysis	15
II-3 Non linear behaviour.....	17
II-3.1 Velocity rate and wavelength.....	17
II-3.2 Power spectra.....	23
II.3.2.1 Comparisons between experimental and numerical results.....	24
II-3.2.2 Power spectra and turbulent behaviour	27
3.2.2.1 Spectra compensation taking into account the spacing between the potential probes	27
3.2.2.2 Taylor's hypothesis.....	28
III-BEFORE CONCLUDING : A GLIMPSE AT 2D-TURBULENCE RESEARCH.....	33
IV-CONCLUSIONS	36
V-REFERENCES	37

INTRODUCTION

A small liquid metal loop called GALINKA has been developed in IATF by L. BARLEON and his team to study magnetohydrodynamic flows [1]. It consists of an integrated horizontal loop exposed to a steady vertical magnetic field of up to two Tesla.

The aim of this work, defined during the early stages of my stay in IATF, was to develop a new GALINKA loop in order to study quasi two-dimensional magnetohydrodynamic flows. More precisely, we use this new loop to prove the model calculations of L. BÜHLER on instabilities driven in a rectangular duct by a non uniform conductivity of the Hartmann wall. The experimental results show good agreement with the analytical predictions, both concerning the linear stability analysis and the non linear calculations based on a quasi two-dimensional magnetohydrodynamic flow model.

First we describe the experimental facility and outline the aim of the measurements. Then we deal with the comparison between the theoretical and the experimental approach. In conclusion we give an outlook on how to use the new GALINKA loop in order to get a better understanding on two-dimensional magnetohydrodynamic channel flows and their interactions with the lateral walls.

I- EXPERIMENTAL DEVICE

I-1 General presentation

Fig. 1 shows a schematic sketch of the loop we built, called GALINKA II. The whole loop is exposed to an uniform magnetic field with an available maximal field strength of 2 T. Roughly speaking this loop consists of four parts.

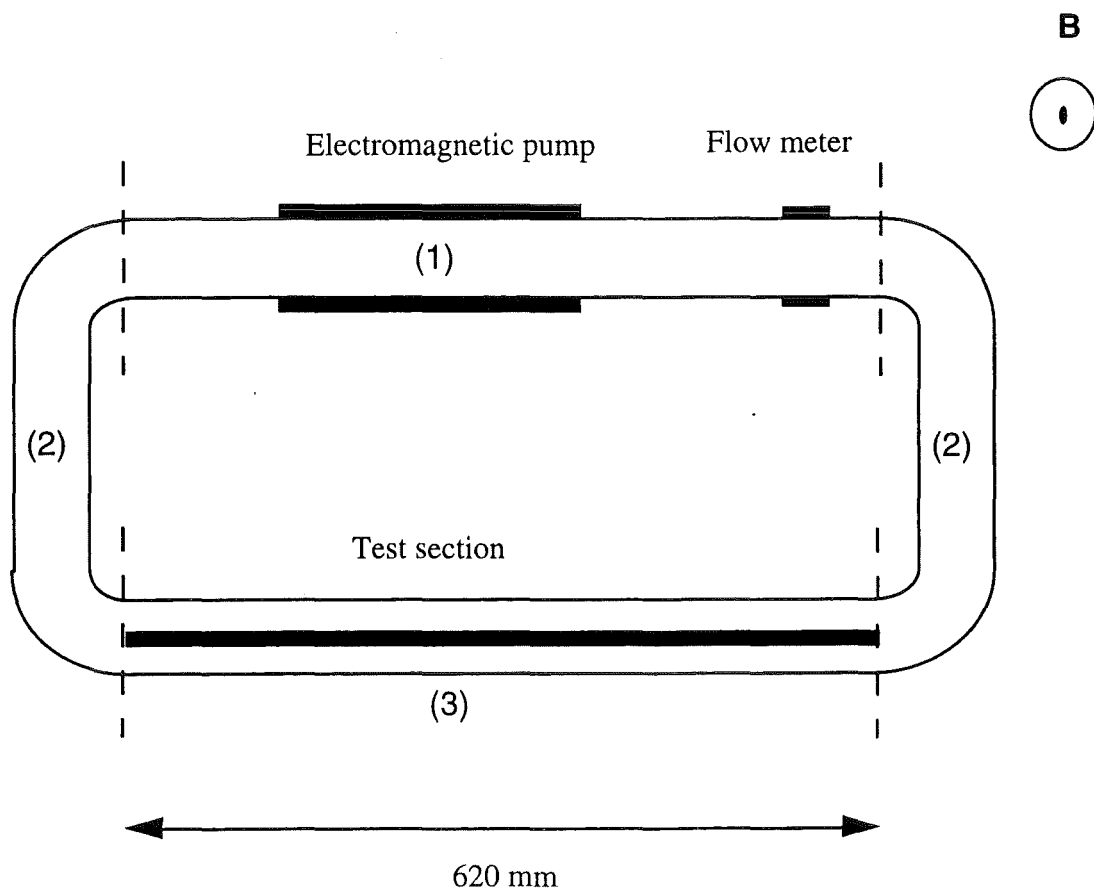


Fig. 1: Sketch of the GALINKA II In/Ga/Sn loop in an horizontal plane. The loop consists of an electromagnetic pump section (1), two return sections (2) and the test section itself (3). The loop is exposed to a uniform steady vertical magnetic field perpendicular to the view plane which can be continuously varied from 0 to 2 T.

-The electromagnetic pump section (1) which is 620 mm long. The conducting pump is made of two copper electrodes 300 mm long embedded in the lateral vertical walls of the section. The pump can be supplied by a D. C. current of 0 to 2000 A, which generates a velocity of up to $2 \text{ m}\cdot\text{s}^{-1}$. A flow meter made of two copper disks, 12 mm in diameter,

inserted in the lateral walls in the same section, gives the mean flow velocity by measuring the voltage gradient.

- Two return sections (2) which close the loop. The bends were designed to be as smooth as possible in order to avoid flow perturbations.

- The test section itself (3), also 620 mm long. It can be easily removed from the loop and replaced by a section of different aspect ratio for the purpose of new experiments. Flow straighteners, made of insulating material, are inserted both at the inlet and outlet of the test section. Each flow straightener is 25 mm long thus the efficient length of the test section is in fact 570 mm. During the study starting September 1994 and ending 1995 we always worked with the same test section. More details on the test section are given in the next paragraph together with an outline of the experiments.

I-2 Aim of the measurements

The study of quasi two-dimensional magnetohydrodynamic flows (hereinafter referred to as quasi 2D-MHD flows) and turbulence promotion by various techniques was first motivated at the IATF by the search for an improvement in heat transfer at the first wall of liquid metal cooled fusion blankets. We underline in the conclusions of this report that the new experimental metal loop also meets the requirements for more fundamental experiments in the domain of 2 D-MHD unstable and turbulent flows.

Several ideas emerged in the seventies on the enhancement of turbulence in 2D-MHD flows. One of these was to promote shear layers in the flow by means of a non uniform conductivity of the Hartmann walls [2]. This non uniform conductivity may be obtained by inserting a conducting strip in the Hartmann wall of an insulated duct and this is what we have chosen. **Fig. 2** shows a cross section of the test section. The section is 60 mm wide and 30 mm high, and is made of a fibreglass reinforced Epoxy, an electrically isolating material. Two strips made of copper, 5 mm wide and 600 mm long are inserted in the middle of the top and bottom Hartmann walls. The strips are 35 μm thick. This thickness has been carefully chosen in order to permit precise comparisons between the experimental results and the calculations performed by L. BÜHLER [3], [4] on this subject.

The principle of the flow destabilisation can be explained as follows. For high Hartmann numbers the flow is bidimensional and divided in two regions, the core region where the current density is constant and the Hartmann layers where the current density depends on the wall conductivity. The induced currents are closing in the cross section of the test section. At the edges of the conducting strip, the electric currents enter the strip leading locally to a lower near-wall current density.

The interaction between the magnetic field and this near-wall current sheet leads to Lorentz forces in flow direction. A friction force, due to viscous effects in the fluid, opposes this Lorentz force. The balance between the two forces defines the final flow velocity.

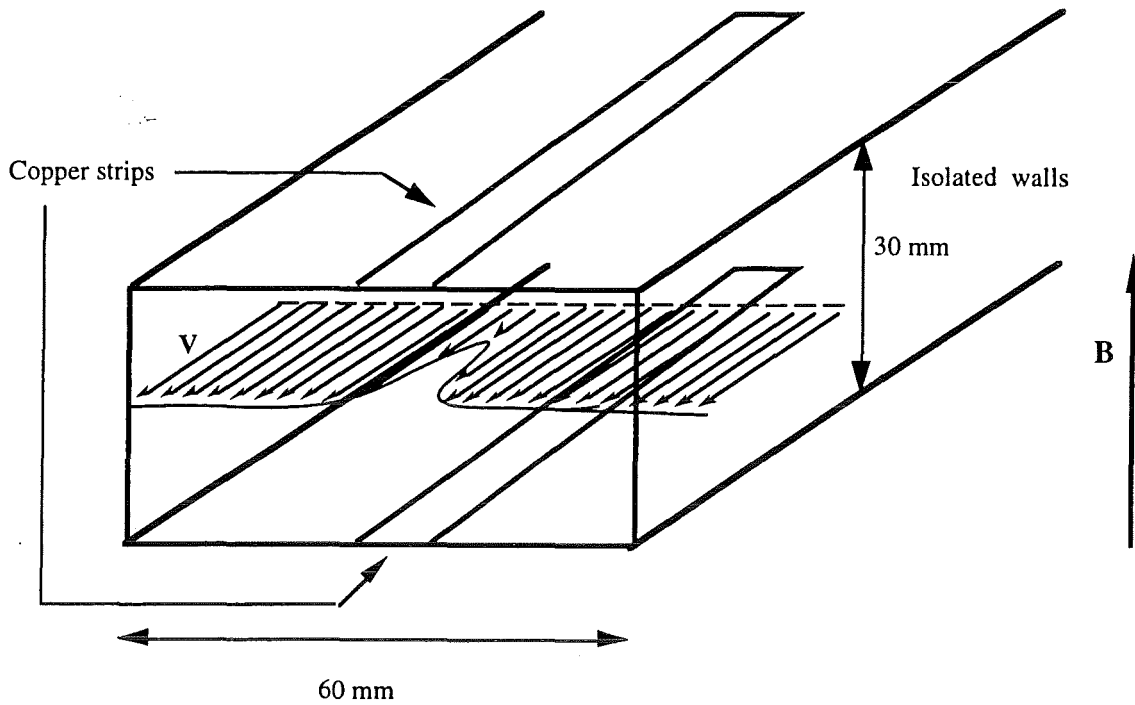


Fig. 2 : Cross section of the test section. In order to decrease perturbations of the flow by the loop itself, the cross section remains the same over the whole loop. This was not the case for the first GALINKA loop. The arrays in the middle plane present the shear velocity profile due to the step of the electrical conductivity in the channel walls.

The velocity is then reduced when the near wall current density decreases by means of an increased wall conductivity. A double shear layer is thus created in the flow by means of the copper strips inserted in the channel. The principle feature of the velocity profile is shown in **Fig. 2**. It can be shown ([3], [4]) that this shear velocity profile with two inflection points may become unstable leading to the formation of a vortex street. We perform potential measurements at the upper Hartmann wall in order to measure the local velocity field and to detect flow instabilities,

I-3 The velocity measurements

In the case of 2D MHD flows the electric potential gradient is linearly related to the velocity in the core of the flow (see for example [5]). Therefore we have developed a potential probe array in order to get a direct "image" of the velocity field generated by the shear flow inside the channel. This array is inserted in the top wall of the test section. The principle design can be seen in **Fig. 3**. In our case we have to encounter a particular difficulty. Because of the weakness of the expected signals at the individual potential probes, the measurements require high precision amplifiers.

I-3.1 Order of magnitude of the potential measurements

As we have mentioned already, the direct current electromagnetic pump is placed, together with the whole loop, in a steady vertical magnetic field, which allows us to achieve a maximal velocity of the order of 2 m.s^{-1} . Measuring the oscillation onset of the spanwise velocity proved to be an excellent procedure for determining precisely the stability threshold of the flow as a function of the Reynolds and the Hartmann numbers.

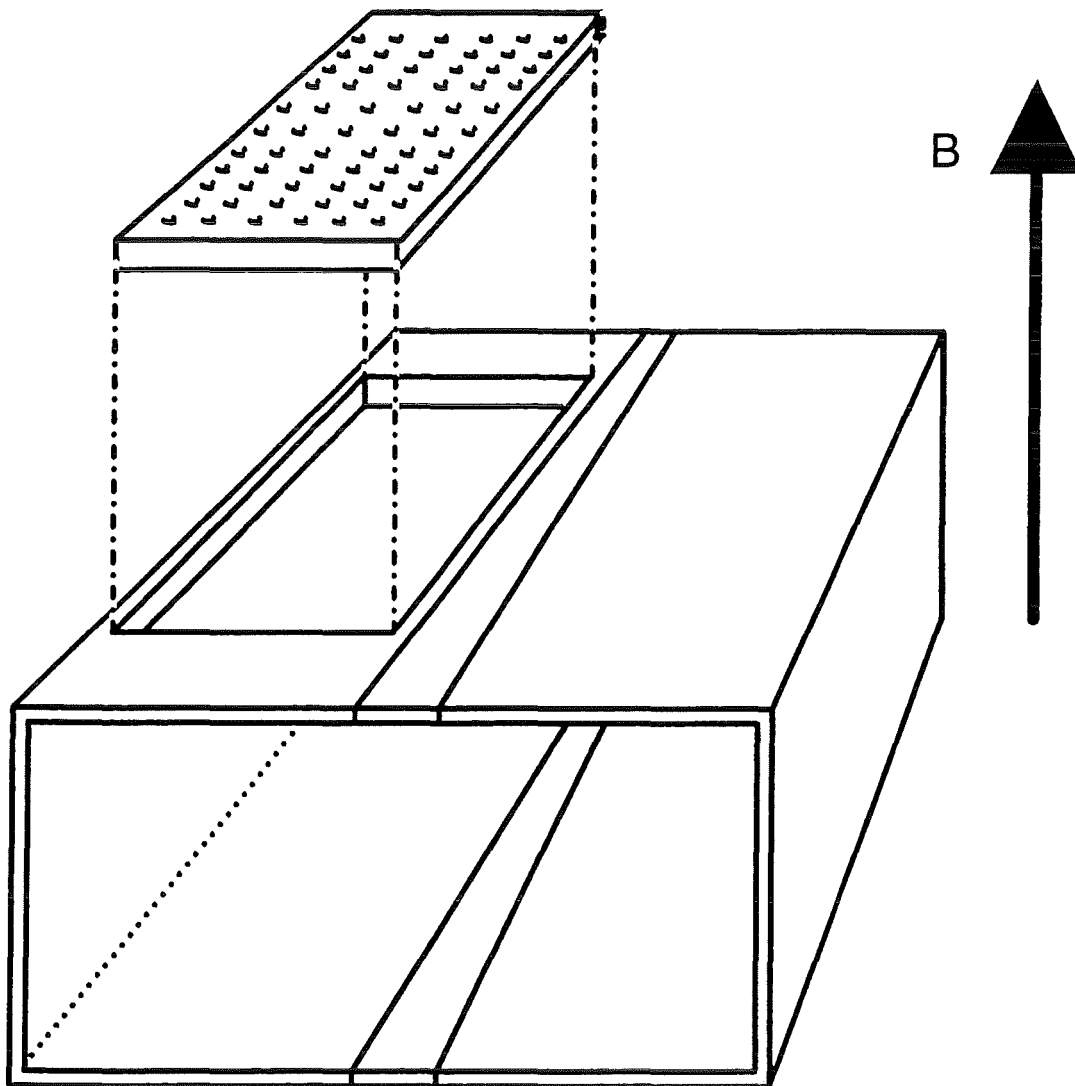


Fig. 3 : The test section and its top removable array of potential probes.

A typical magnitude of the electrical potential to be measured is given by :

$$\Delta\Phi = \Delta X * B * V,$$

taking : $V = 10 \text{ mm.s}^{-1}$ and $B = 1 \text{ T}$, we get $\Delta\Phi = 0.01 \text{ V.m}^{-1}$. The choice of the best spacing ΔX between two consecutive probes is the result of a compromise. On the one hand it should not be too small in order to get a measurable signal, which is not too noisy, and on the other hand it should not be too large in order to have sufficient precision on the local velocity measurements related to a given structure in the flow. We finally used a spacing of 2.5 mm. This gives a typical order of magnitude of $25 \mu\text{V}$ for the potential measurement. This is an acceptable value considering that in our case we are only performing isothermal measurements so that the signals are not subject to additional thermo-electric effects occurring in the measurement circuit. We developed two arrays of probes with this spacing. The first one with 23 probes is arranged in two rows of 10 probes in the flow direction and of three additional probes in the transverse direction. **Fig. 4** displays the location of the 23 probes in the test section.

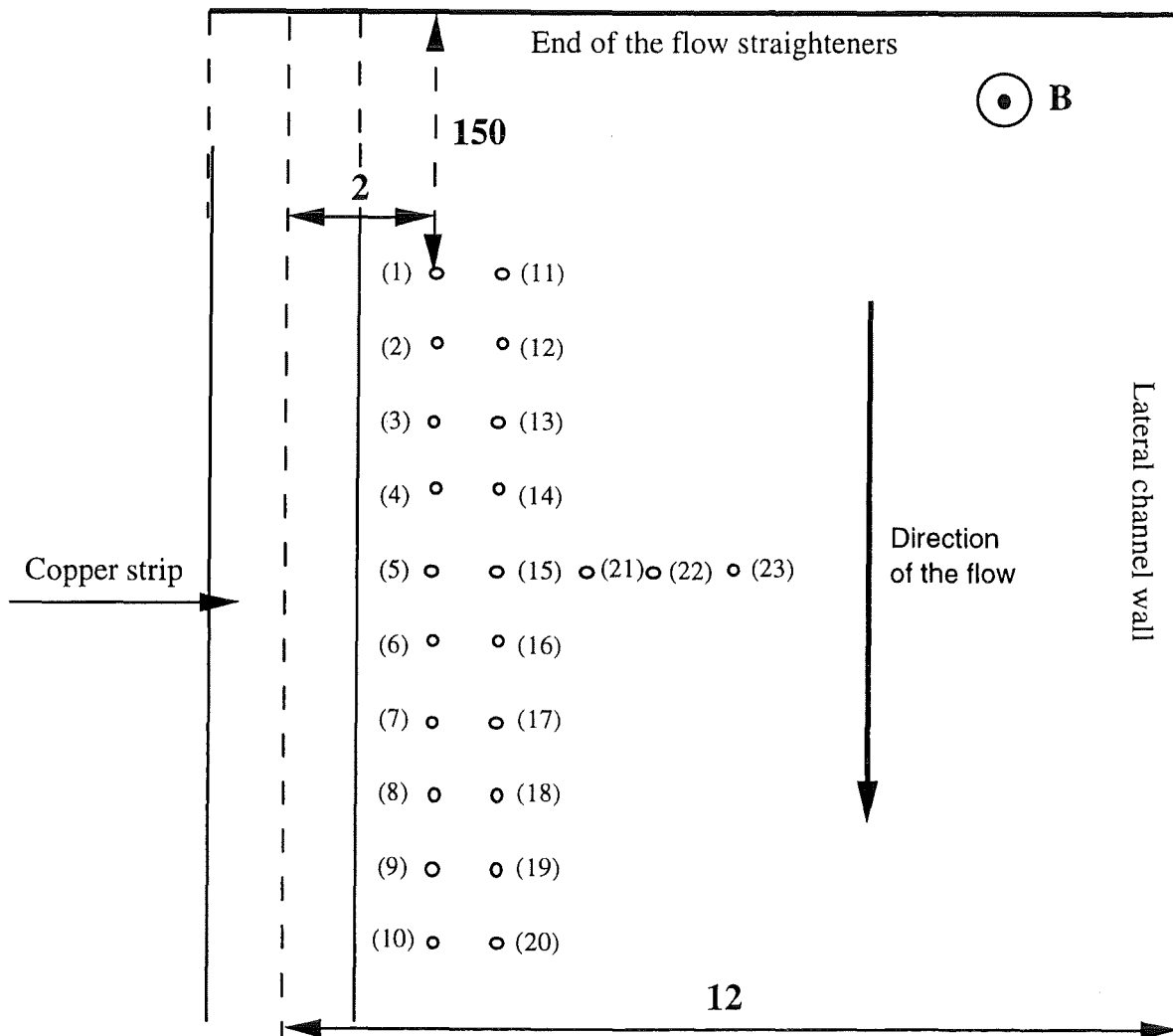


Fig. 4 : Location of the probes in the 23 potential probe array (top view). The distances indicated on this scheme are non dimensionalized by the spacing of 2.5 mm between two probes, which is also equal to the half width of the copper strip.

All the results reported here have been obtained with this first array. **Fig. 5** shows a photograph of the second array with 6*11 probes. We use the same technique as for the first array. Thus each probe is made of one miniature coaxial heater rod. Only the inner nickel wire with diameter 0.1 mm is in contact with the liquid metal. The only difference between the two arrays concerns the common mass wiring. This point leads us to discuss the problem of the signal amplification in the next section.

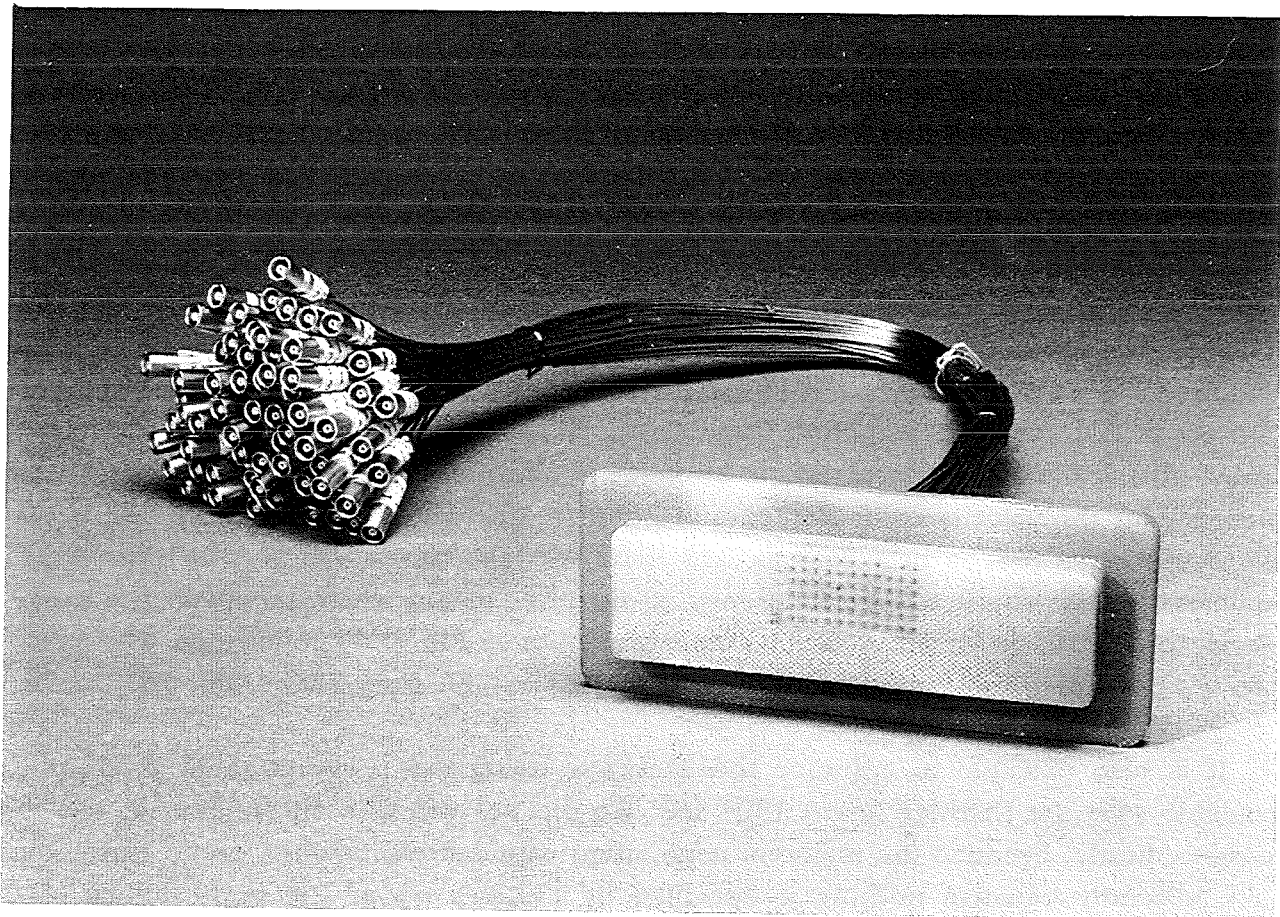


Fig. 5 : A photograph of the 6 X 11 potential probe array.

I-3.2 Amplification of the signal

Ten amplifiers were used together with the 23 probe array. These amplifiers had generously been lent by R. BOLCATO from the laboratory EPM-MADYLAM in GRENOBLE to enable us to get the first experimental results more quickly. Most of the measurements consist of potential measurements between two consecutive probes in a truly differential manner which helped to eliminate the common mode noise. We also tried to perform measurements with a common potential for the sheaths using these amplifiers and this specific array but the noise level was too high. This outcome was due on the one hand to the fact that no clear common potential was available and on the other hand to the fact that the amplifiers seem to be too sensitive to the environment (perhaps there was a

problem of separation from the electrical network). Nevertheless the use of those amplifiers helped us to define the requirements for a new generation of amplifiers developed in IATF by R. VOLLMER. Four of these new amplifiers have been already tested with the 23 probe array both for true differential and common ground measurements. In both cases the results are satisfactory though the common ground used for the preliminary measurements was not as good as expected for the 6*11 probe array. Hence for the latter a "star wiring" was performed in order to avoid perturbations. For this purpose each coaxial wire passes through a hole made in a copper plate of 5 mm thickness which lies directly on the probe array. Thus the electrical contact between the shield of each coaxial wire and the copper plate is ensured. One of the most central probes of the array is taken as common ground and is then directly welded to the copper plate.

Each of the coaxial wires is linked to the input of its attached own amplifier. The output of each amplifier, (the gain is set at 500), is connected to a data acquisition board : a DAS 1801 HC board from Keithley driven by a 486PC. This board is configured with either 64 single-ended or 32 differential analogue input channels depending on the input configuration specified in the configuration file. The analogue input range in the bipolar mode is +/- 5 V. That leads to a maximal accuracy of 4.88 μ V when taking into account the gain set at 500 for each amplifier. Considering the fixed spacing of 2.5 mm between two probes this leads for a characteristic strength of the magnetic field of 1 T to a maximal accuracy for the velocity measurements of 2 mm/s. The maximum sampling rate between two consecutive probes in a scan is 312 KHz. We take advantage of this high value as compared to the characteristic frequency of our phenomena which is within the range of 10 Hz, to perform quasi simultaneous measurements as **Fig. 6** demonstrates. The software used for acquiring and processing the data is "TEST POINT" from CEC under WINDOWS.¹⁾

1) It is also possible to enhance the accuracy using the programmable internal gain available with the Keithley board 1801 HC. We did not use this alternative for two main reasons, firstly, because the maximal acquisition rate decreases when using this internal gain, secondly because nothing is specified by Keithley about the performance of this internal amplifier.

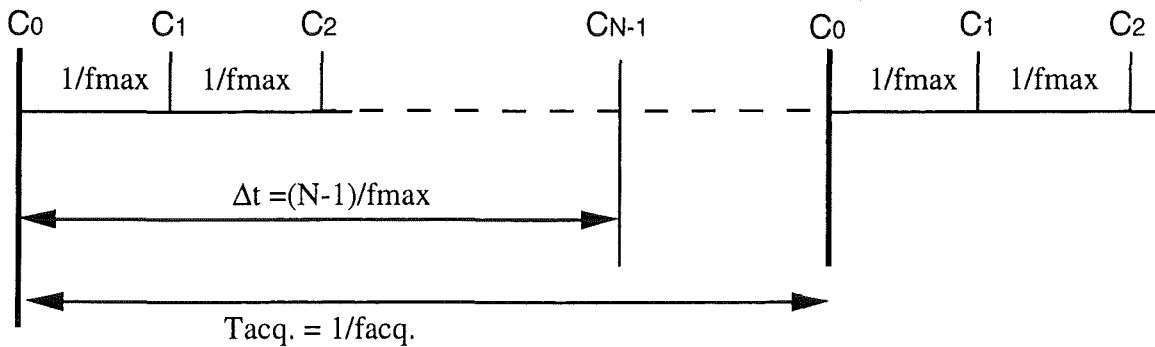


Fig. 6 : The quasi simultaneous measurements. In the so called "burst mode" the user defines only the time spacing between the beginning of two consecutive scans while the N consecutive channels are acquired within a time $\Delta t = (N-1)/f_{max}$, f_{max} being the maximal acquisition rate depending on the board used, 312 KHz in our case. The quasi simultaneous measurements are achieved only if the product R of the physical phenomenon characteristic frequency (10 Hz) with Δt is small. The worst case is given when the 64 channels are acquired for purpose of "visualisation", but even in this case we have $R = 2 \cdot 10^{-3}$.

I-4 Summary

The aim of this first chapter was not to give a complete technical presentation of the experimental facility we built. For more details one should refer to the file entitled "GALINKA II" available from K. J. MACK to whom I am very grateful for the construction of the loop. In the following section we will outline the associated technical problems wherever needed for understanding a particular result.

The most important feature to be emphasised in this technical description is that GALINKA II provides a new flexible loop to investigate MHD flows. Its particular appeal is that the test section can be easily removed and replaced for the purpose of new experiments, (e.g. : multi-channel investigations, interactions between vortex and lateral walls and so on). Moreover the instrumentation (two different probe arrays are available) can be easily inserted in these new test sections.

II EXPERIMENTAL RESULTS

In this section we compare our experimental results with the analytical ones obtained for the same configuration. These analytical results consist on the one hand of a linear stability analysis and on the other hand of non linear calculation based on a quasi 2D flow model. The relevant model has been developed by L. BÜHLER [2,3] at the IATF. Before reporting and discussing the results we will focus on the related dimensionless numbers we use.

II-1 Dimensionless characteristic numbers

As in the notation used in [3,4] Re , Ha , and N denote respectively the Reynolds number, the Hartmann number and the Interaction parameter based on the half width of the copper strip (L) :

$$\begin{aligned} Re &= (L V)/\nu \\ Ha &= B L (\sigma/\rho\nu)^{0.5} \\ N &= Ha^2/Re \end{aligned}$$

We use also the rescaled Hartmann number, denoted M , based on the half channel height. Defining "a" as the ratio between the height of the channel ($2D$) and the copper strip width ($2L$), we have the relation:

$$M = a Ha.$$

Another important parameter is the conductance ratio "c" which compares the wall conductance to the liquid metal conductance:

$$c = \frac{d\sigma_{wall}}{D\sigma_{metal}}$$

where "d" is the thickness of the conducting part of the Hartmann wall (the copper strip). In our loop the liquid metal used is the In/Ga/Sn alloy, so that we have for all experiments:

$$\begin{aligned} \sigma &= 3.27 \cdot 10^6 \Omega.m^{-1} \\ \nu &= 0.34 \cdot 10^{-6} m^2.s^{-1} \\ \rho &= 6360 kg.m^{-3} \end{aligned}$$

The three values are given for 25 °C.

The geometrical dimensions are :

$$\begin{aligned} D &= 15 \text{ mm} \quad (\text{the half channel height}), \\ L &= 2.5 \text{ mm} \quad (\text{the half copper width}), \\ a &= D/L = 6 \quad (\text{the aspect ratio}), \\ d &= 35 \text{ } \mu\text{m} \quad (\text{the copper strip thickness}). \end{aligned}$$

This leads for all our experiments to a conductance ratio: $c = 0.04$. The choice of the copper strip thickness that leads to this value for c is the result of a compromise which we will explain. As presented in [3], the characteristic time scale for the decay of vorticity due to Joule's dissipation, can be expressed:

$$\tau = \frac{1}{N} \left[\frac{1}{M} + \frac{c}{1+c} \right]^{-1}$$

when taking into account the finite conductivity of the walls. We have then:

$$\text{for } c \ll M^{-1} \quad \implies \quad \tau = M/N \quad (1) \quad (\text{classical for insulating walls})$$

$$\text{for } M^{-1} \ll c \ll 1 \quad \implies \quad \tau = (cN)^{-1} \quad (2)$$

$$\text{for } c \gg 1 \quad \implies \quad \tau = N^{-1} \quad (3)$$

This last limit of the relation (3) indicates that, for high interaction parameters, vortices resulting from instability will be damped quickly when choosing a copper strip which is not too thick. In contrast, when a moderate value is chosen, this leads to a value of c in the range expressed in relation (2) that permits the observation of vortices even for large interaction parameters. In our case we have

$$0.001 \ll M^{-1} \ll 0.004, \quad \text{so that :} \quad M^{-1} \ll c = 0.04 \ll 1.$$

Thus, from an experimental point of view, once c is fixed, the only two parameters which can be varied are the velocity of the mean flow by means of the electromagnetic pump and the strength of the steady vertical magnetic field strength.

II-2 Comparison with the linear analysis

Fig. 7 displays the marginal stability curve in the (Re, M) plane.

The Re_c curve gives the dependence of the critical Reynolds number for the onset of the instability for increasing values on the rescaled Hartmann number M .

The $S_{r,c}$ curve is the real part of the eigenvalues and corresponds to the phase velocity. The subscript "c" stands for "critical" which means that the imaginary part of S , noted S_i , is then equal to zero. $S_{r,c}$ is in fact equal to the propagation velocity of the perturbation.

The k_c line gives the dependence of the critical wave number on M . Again the imaginary part of k is equal to zero at the onset of the instability. This wave number is normalised by the half width of the copper strip. We then have $k = k_{\text{exp}} L$. Hereinafter the subscript "exp" will be related to an experimental dimensional value and the lack of subscript to a non dimensionalized value.

The points that can be seen on the curve are obtained from the experimental values of electrical potential. In the next section we focus on the procedure with which they have been obtained.

II-2.1 Threshold of instability

Fig. 7 displays three critical Reynolds numbers corresponding to $M = 300$, 566 and 1000 . We have to stress that the value of $M = 1000$ is already close to the maximum value achievable. The maximum magnetic field strength of $2T$ gives $M = 1167$ and this is the upper limit of our experimental investigations. As far as the lower limit is concerned, we did not perform measurements for $M < 300$ because the signal was then at the lower operational limit of the first generation of amplifiers.

Theoretically, the velocity fluctuations in transverse and axial directions tend to zero when reaching the critical Reynolds and Hartmann number starting from supercritical values. Searching experimentally Re_C at which the fluctuations are zero is impossible because the signal becomes too small and it is thus impossible to retrieve the signal clearly from the background noise. Therefore, for each value of M we performed a series of experiments with increasing Re . We calculated the standard deviation of the transverse velocity obtained from potential measurements. The extrapolation of the best fit curve gives the value of the critical Reynolds number. **Fig. 8** displays such a curve for $M = 566$. A linear extrapolation of this curve gives an approximate value of Re_C . In this case $Re_C = 284$.

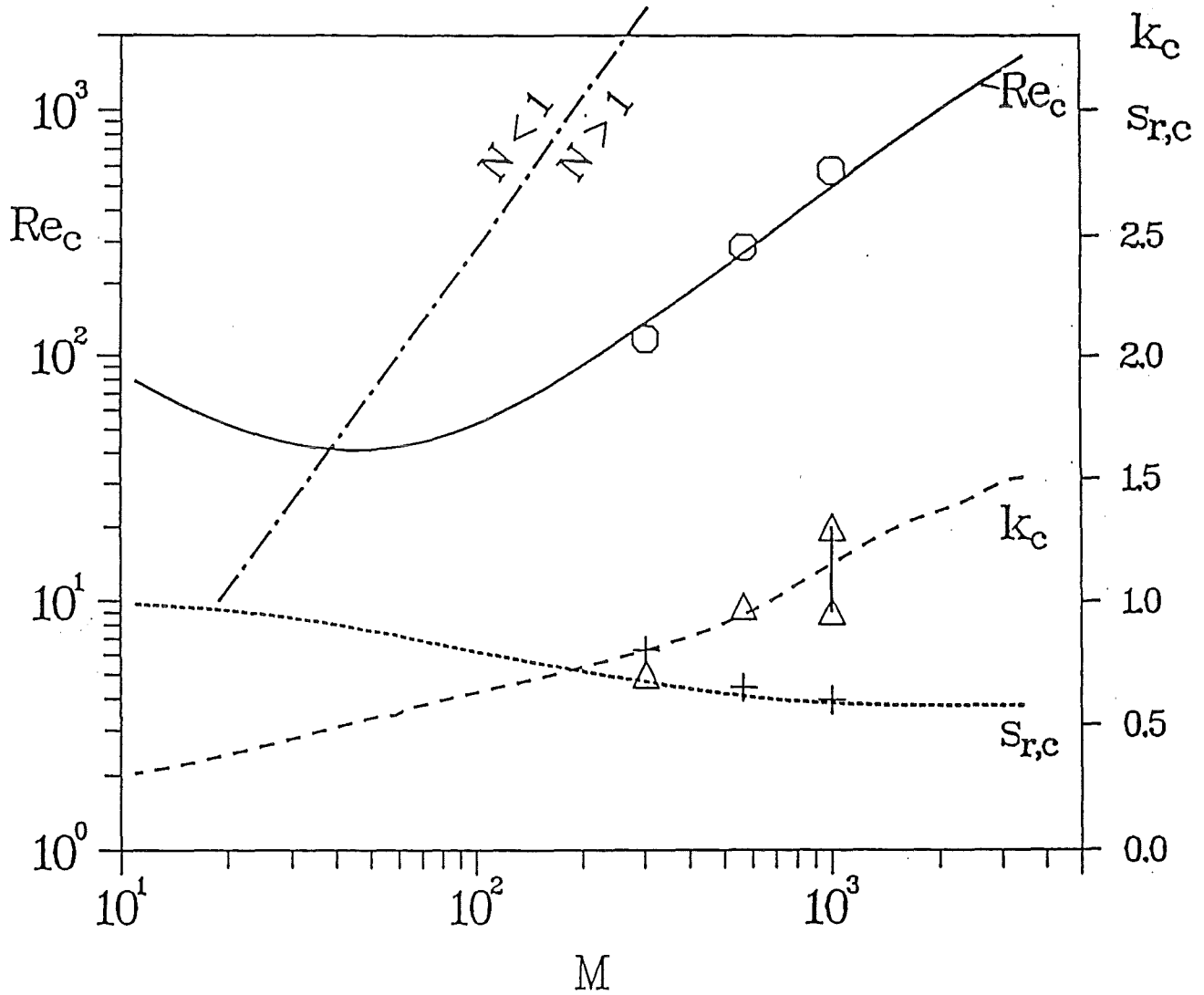


Fig. 7 : The stability limit for GALINKA II, $c = 0.04$ and $a = 6$.

Re_c : critical Reynolds number, k_c : critical wavenumber, $S_{r,c}$: critical ratio of the perturbation propagation to the mean velocity. Lines are according to the linear theory, symbols represent experimental values.

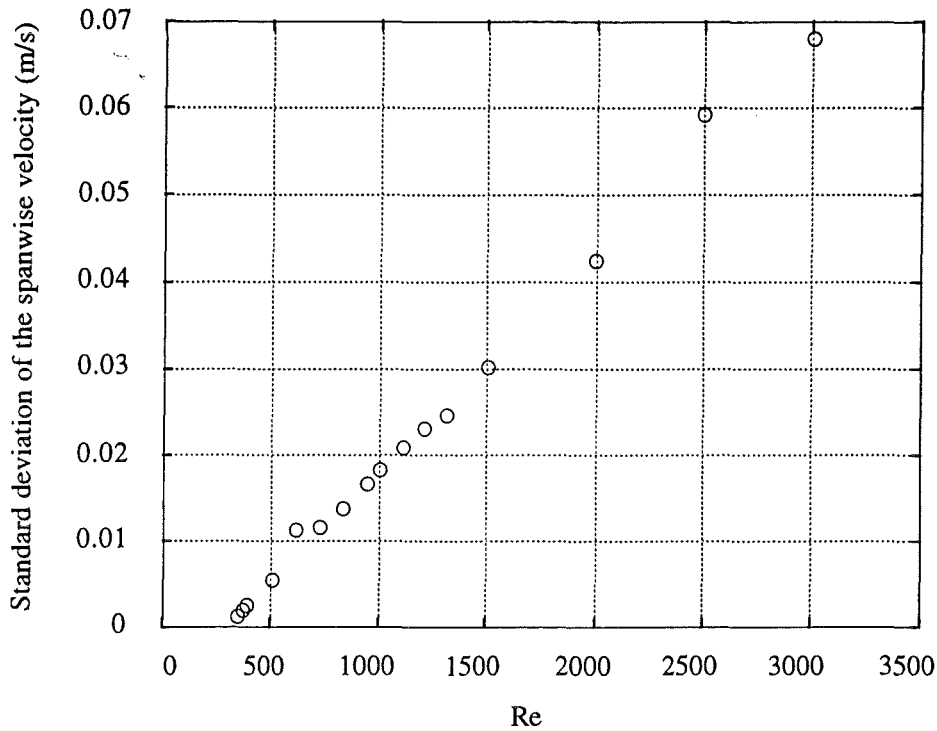


Fig. 8: The standard deviation of the transverse velocity as a function of the Reynolds number based on the measurement of $\Delta\Phi_{1,2}$ for $M = 566$. A linear extrapolation of this curve leads to $Re_c = 284$.

II-2.2 Calculation of the critical propagation velocity

We call "propagation velocity" the speed at which the perturbations of the flow travel downstream. It is calculated by performing a cross correlation between two signals coming from different probes located on the same streamwise axis. Most of the time, the cross correlation is made between the probes as indicated in **Fig 4** : $\Delta\Phi_{1,2} = \Phi_2 - \Phi_1$ and $\Delta\Phi_{9,10} = \Phi_{10} - \Phi_9$. The spacing between two measurements is then 2 cm. Again, because of the extremely low intensity of the signal, it is impossible to get a direct measurement of the propagation velocity just at the critical Reynolds number. So the propagation velocities are evaluated for slightly supercritical values of the Reynolds number. As we will see in § II-3, the propagation velocity increases with the Reynolds number, so that the results we display here are certainly overestimated.

II-2.3 Calculation of the critical wave number

The instability occurs with a defined wave number. To determine this experimentally, we need on one hand the propagation velocity (obtained in the way we have

just described) and on the other hand the characteristic frequency of this instability. We have then:

$$k_{\text{exp.}} = \frac{2\pi}{\lambda_{\text{exp.}}} = \frac{2\pi f_{\text{exp.}}}{V_{\text{exp.}}}$$

There is naturally a greater uncertainty for this derived quantity than in the two previous cases. There are two reasons for this. First this quantity is derived from measured quantities and secondly the determination of the perturbation frequency $f_{\text{exp.}}$ is difficult. Hence to obtain a readable spectrum we are forced again to consider values of Re greater than the critical value. Unfortunately the spectrum then already contains several dominating frequencies due to non linear effects. This explains the two values that we give for k_c for $M = 1000$ in **Fig. 7**. The spectrum used to determine these values is shown in **Fig. 9**.

II-2.4 Conclusion for the comparison between the results and the linear analysis

Despite the small range of M investigated, we find good agreement between the analytical approach of the linear stability analysis of the flow and the experimental results. For the particular measurements we have to recall that we performed only 10 quasi simultaneous measurements so that we are not able at this stage to extract images of the vortices from the data. Nevertheless the physical quantities we determined show that these vortices exist and can be traced. This proves moreover that the choice of the conductivity parameter "c" was correctly chosen, the damping is not too strong and that the main perturbation of the flow is indeed caused by the copper strip. It has been demonstrated thoroughly that the flow straighteners are efficient in homogenising the flow downstream of the bends in the loop.

It is further of great interest to succeed in performing measurements at a lower value of the Hartmann number. Hence we choose a lower value of the interaction parameter. **Fig. 7** displays the frontiers where the interaction parameter, N , is equal to unity. Normally, the linear analysis is only valid in the range $N \gg 1$, assuming 2D flows. Approaching this limit we will be able to detect some deviations from the theoretical predictions, which would be in fact the indication of an increasing three-dimensional behaviour.

For the time being we use the linear analysis as a guide to interpret our results. We will now display some results beyond the stability limit. These results can be compared with analytical and numerical results, but as we shall see, it will now be more difficult to make comparisons for two main reasons. Firstly, because of the presence of lateral walls which are not fully taken into account by the model and secondly because of a high Reynolds numbers. For some values of M , which have been studied, the interaction parameter becomes low and the divergence between the experimental and theoretical approaches should indicate the limitation of the two-dimensional model.

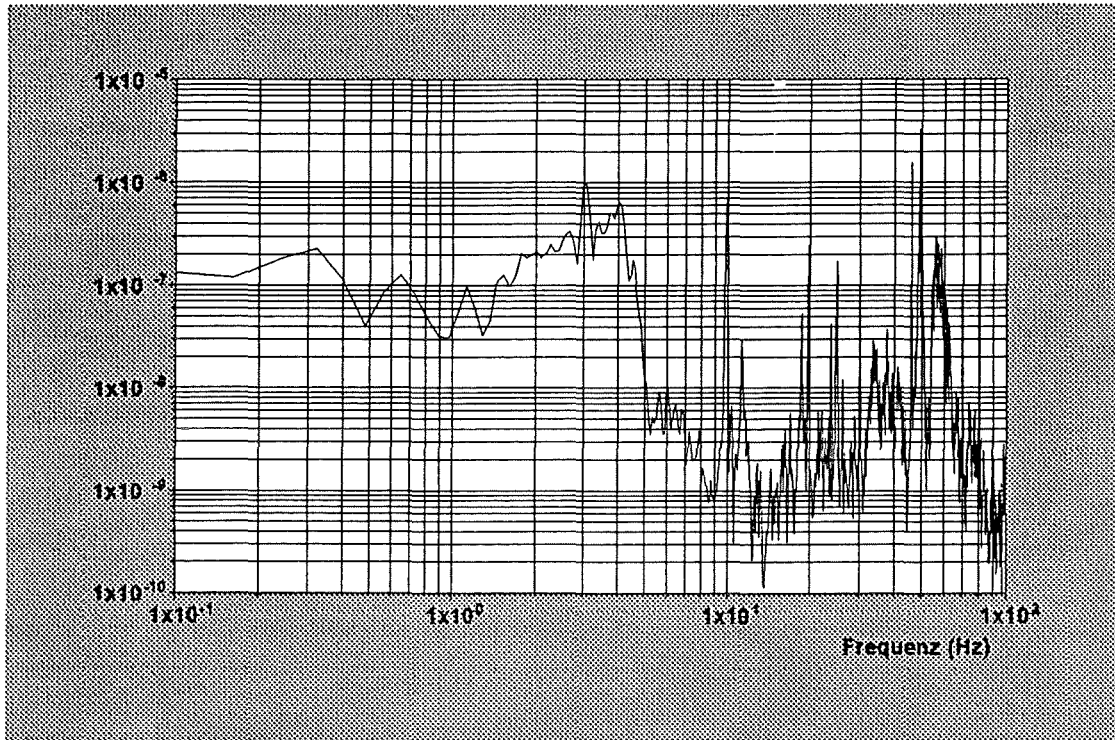


Fig. 9 : Power spectrum of the transverse velocity for $M = 1000$, and $Re = 594$. The acquisition frequency is $f_{acq} = 330$ Hz, and the amount of data 8192. This spectrum shows the difficulties encountered when performing measurements near the critical Reynolds number. For this value we notice two dominants peaks at 3.1 and 4.1 Hz. This signal is non-filtered and therefore we find a sharp peak at 50 Hz. The other spurious peaks seem to be related to aliasing phenomena. Hence the acquisition frequency is only 330 Hz which is not enough to take into account the parasitic frequencies coming from the magnetic field power supply. These frequencies were noted to be harmonics of 150 Hz during preliminary tests performed with a higher acquisition frequency.

II-3 Non linear behaviour

In a first part we display and discuss, the evolution of the ratio of the propagation velocity to the mean velocity, (hereinafter referred to as velocity ratio), and of the wavelength as a function of the Reynolds number. We investigate this dependency for three different values of M . The second part deals with the power spectra obtained from our experiments.

II-3.1 Velocity ratio and wavelength

Fig. 10, exhibits the variation of the velocity ratio with the Reynolds number for $M=300$, $M= 566$ and $M = 1000$. In the three cases this ratio can be seen to increase for increasing Reynolds numbers. It is noteworthy that the velocity ratio variation obtained for the lowest M is somehow different from the two others. Hence, for the two larger values the ratio reaches at the critical Reynolds number the value predicted by the linear analysis, close to 0.6. This can also be seen on **Fig. 7**. In contrast the ratio is higher than predicted for the case $M=300$. We will interpret this discrepancy after presenting the variation of the wavelength with the Reynolds number.

Fig. 11 gives the wavelength variation with Reynolds number for $M=300$, $M= 566$ and $M = 1000$. In the three cases the characteristic wavelength of the perturbation is increases for increasing Reynolds numbers. For the three cases we observe a change in the variation above a critical value for the wavelength. This non dimensional critical value is about 15. The change is particularly dramatic with the lowest value of M , namely $M = 300$. In this case the wavelength starts to decrease for a certain range of Re . In the other two cases the slope of the variation is reduced significantly beyond this critical wavelength.

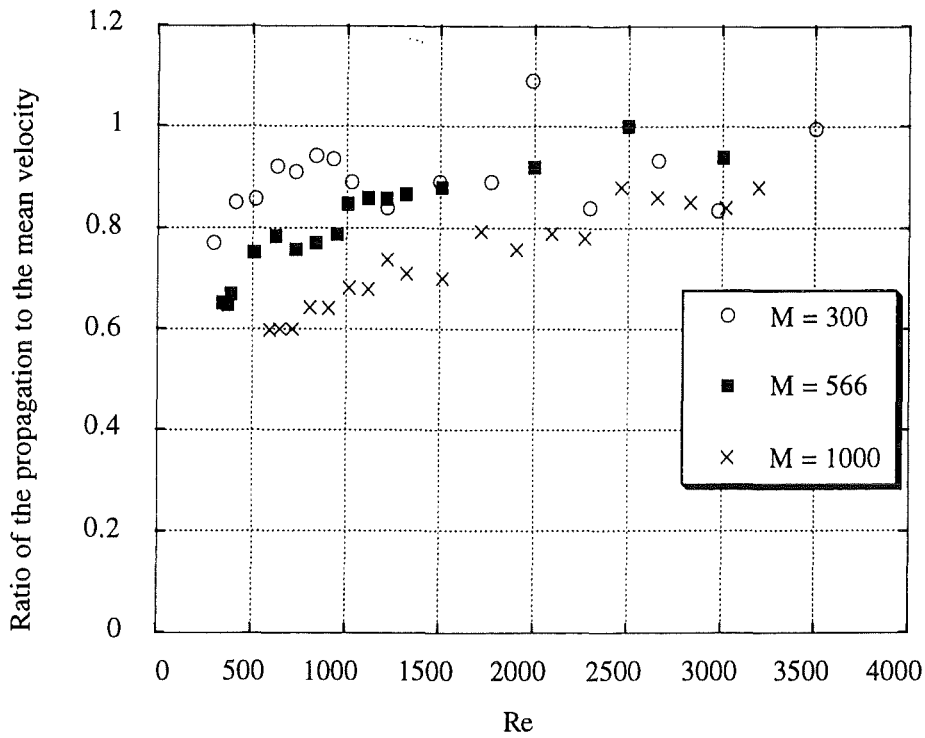


Fig. 10: Ratio of the propagation velocity to the mean velocity as a function of the Reynolds number. $M = 300, 566$ and 1000 .

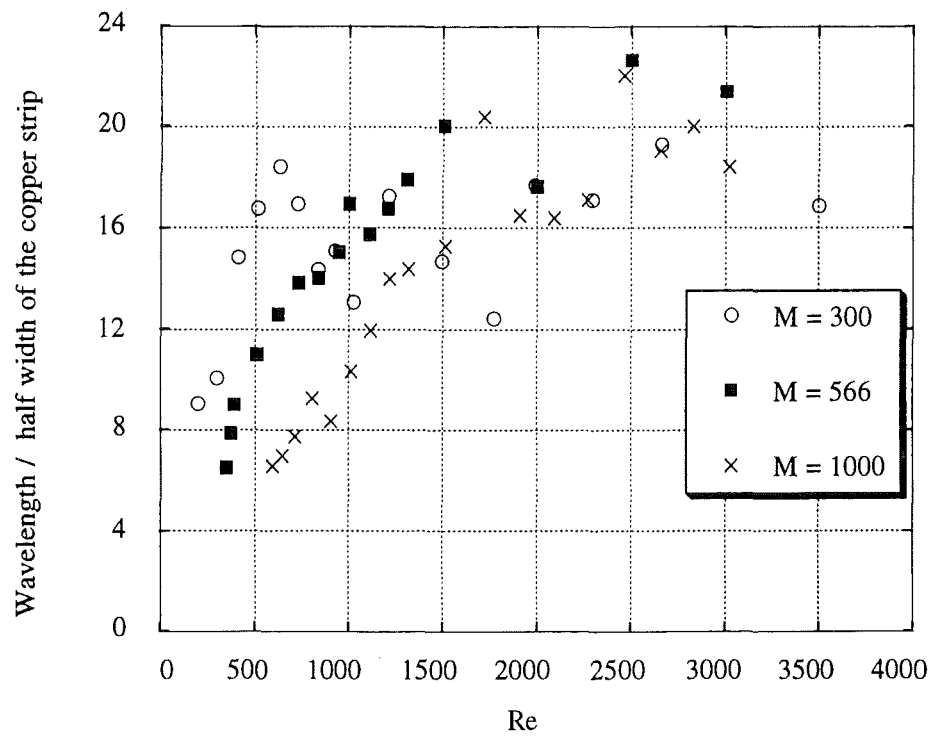


Fig. 11: Characteristic wavelength of the instability as a function of the Reynolds number. $M = 300, 566$ and 1000 .

In order to explain the phenomena we observed, we have to be precise about what we mean by the measurement of a characteristic wavelength associated with the pair of parameters (Re, M) . For this purpose, we first display a numerical calculation performed by L. Bühler with his quasi 2D-MHD model for high interaction parameters. Hence **Fig. 12** gives an instantaneous iso-vorticity pattern in the test section for $(Re, M) = (1000, 566)$. The origin of the coordinate system on the left corresponds to the end of the flow straightener in the experimental set up. The ordinate origin is taken in the middle of the copper strip.

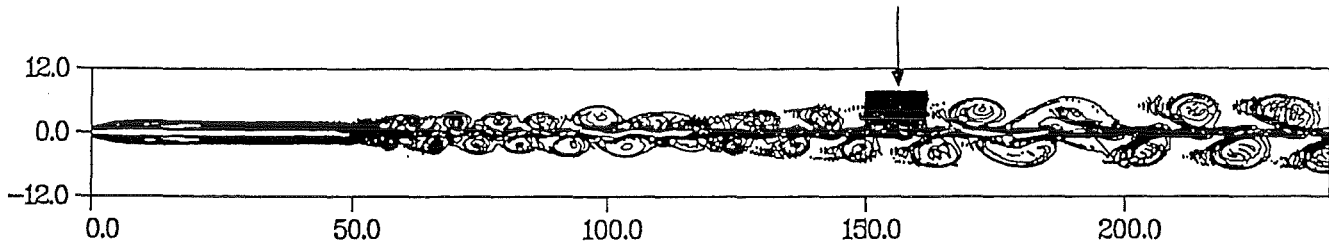


Fig 12 : Chart of the vorticity in the test section as computed by the quasi 2D model of L. BÜHLER for $Re = 1000$ and $M = 566$. The physical test section length (between the two flow straighteners) is 228. The rectangular shape on the graph indicates the array probe location for most of the experiments (measurements between 150 and 158). Using the experimental opportunity to reverse the flow we also performed some measurements between 70 and 78. Then we were able to check the wavelength increase in the flow direction for a fixed couple of parameter (Re, M) .

As we can see from this pattern, the wavelength increases in the direction of the flow from left to right. The black rectangular marker, indicated by the vertical arrow, shows the place where the probe array is located for most of the measurements. We see that we measure a wavelength at a defined place. It can be assumed that the wavelength remains constant across the extent of the probe array. Nevertheless, the spatial evolution of the wavelength demonstrated by this calculation was checked by means of an additional experiment. Since it was impossible to change the probe array location, we reversed the power supply of the electromagnetic pump. The resulting reverse flow permits us to measure a mean wavelength at a distance from the origin between 70 and 78, instead of 150 and 158 as in the previous case. We then compare these experimental results with the calculation. The numerical calculation gives for the two locations

$$\lambda_{70} = 8 \quad \text{and} \quad \lambda_{150} = 15 \quad \text{respectively}$$

As far as the experimental results are concerned we find

$$\lambda_{70} = 11 \pm 1 \quad \text{and} \quad \lambda_{150} = 16.5.$$

The uncertainty found for 70 originates from the fact that the associated experimental time spectrum exhibits three peaks which are of the same order of magnitude for the pair of parameters (Re, M) considered here. Nevertheless we can conclude that this additional experiment confirms in general the wavelength growth in the flow direction.

To summarise, we can say that because of the convective nature of this instability, for given parameters (Re, M) , the characteristic wavelength increases from the critical size to a maximum value controlled by the distance between the copper strip and the lateral wall. This observed phenomenon agrees well with the basic tendency of general 2D-turbulent flows to initiate the emergence of bigger and bigger structures.

In order to understand what the dominant parameters are which govern the change in the wavelength for increasing M or Re we show in **Fig. 13** the wavelength as a function of the parameter Re/M which is the characteristic Joule's dissipation time. In fact this parameter is found to depend on the conductivity of the Hartmann wall as seen in § II-1. However we are dealing here only with the limit of non conducting walls. This model assumption is justified because in the non linear case the major part of the vortex is no more under the influence of the central copper strip.

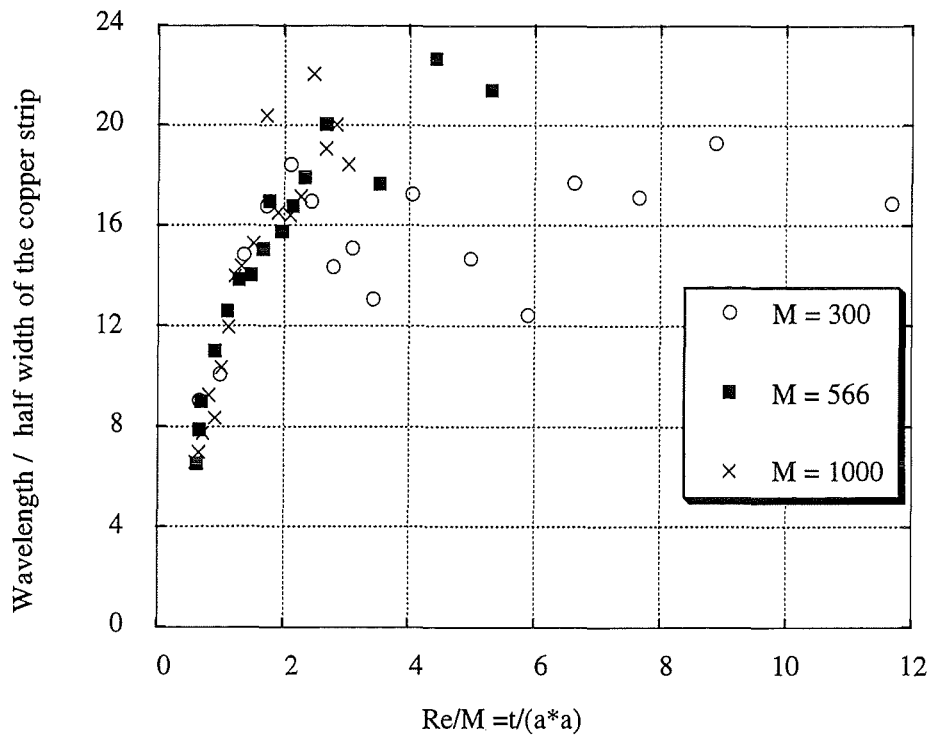


Fig. 13 : Wavelength as a function of the parameter $Re/M = M/N$, the characteristic time for Joule's friction for insulating wall.

The diagram reveals a nearly linear dependence between the wavelength and the Joule's dissipation time below a wavelength threshold which is about 13. Therefore we conclude that the growth rate of the wavelength is controlled mainly by the friction due to Joule effects at least below the threshold. Above this particular value the wavelength can increase further but at a lower rate. This is at least observed for the case of $M = 566$ and $M = 1000$. As the wavelength threshold is very close to the half width of the channel (12), we can suppose that the change in the Re/M -dependence is the consequence of the onset of a possible interaction with the lateral walls.

As far as the peculiar behaviour for $M = 300$ is concerned, we believe that it may be explained by a breakdown of the quasi 2D-behaviour. For this value of M , the experiments are performed for Reynolds numbers in the range 300 to 3000. This corresponds to a range of interaction parameters N between 8.3 and 0.83. Keeping this low range in mind, we can explain the higher velocity ratio observed in this case as compared to the theoretical one by a purely hydrodynamic analogy. Let us assume a 2D hydrodynamic vortex near a wall as shown in **Fig. 14**. Given the distance "a" between the vortex and the wall and a vorticity " Γ " for the vortex considered it can be shown (see [6] for a review on the problem of vortex interactions with walls) that the ratio of the propagation velocity to the outer flow velocity is given by

$V_a/U_0 = 1 - \Gamma/(4 a U_0)$, if the vortex rotates in the way indicated **Fig. 14**, and

$V_a/U_0 = 1 + \Gamma/(4 a U_0)$, in the other case.

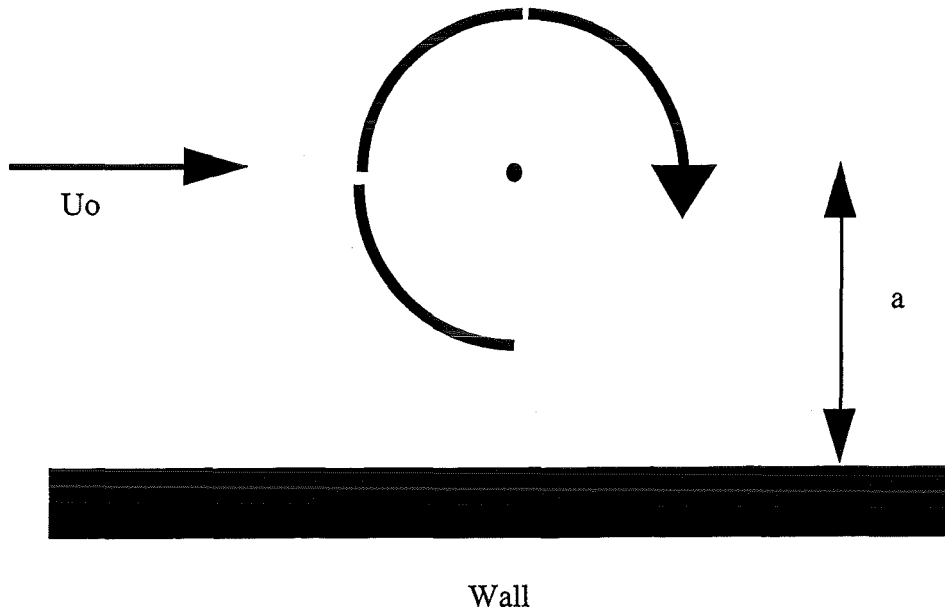


Fig 14 : Diagram of a vortex in a uniform flow above a rigid wall.

It means that in the first case the vortices propagate with a lower velocity than the flow velocity. Then one obtains for a particular distance a : the bigger the vorticity, the slower is the propagation velocity. Let us apply this result to the interaction of the vortex with the copper strip.

Of course in this case there is no wall anymore but the velocity under the copper strip is nearly zero because of the Joule dissipation so that the same kind of phenomenon might occur as in the case of rigid walls. The shear layers generate vortices which rotate the way indicated in **Fig. 14**, when replacing the wall by the edge of the copper strip. Then, it is not surprising that the propagation ratio we measured is smaller than 1. But in the case of small interaction parameters, when the breakdown of the 2D model can be assumed, the 2D model will overestimate the vorticity of a given vortex, leading to an underestimation of the propagation velocity by the theory. This may explain the discrepancy that can be directly seen in **Fig. 7**. Continuing with the same point of view, we can say that when the size of the vortices reaches the half width of the channel they can interact strongly with the lateral wall. This time the interaction will lead to a higher propagation velocity than that of the flow. This phenomena will lead to a strong deformation of the vortex. Again this is more easily observed in the case of low M number where the maximum size of the vortex is reached for a lower Reynolds number. We think that this phenomenon can explain the difficulties we encountered when measuring a defined wavelength in the case $M = 300$ for the highest achievable values of the Reynolds number. **Fig. 15** sums up this last idea.

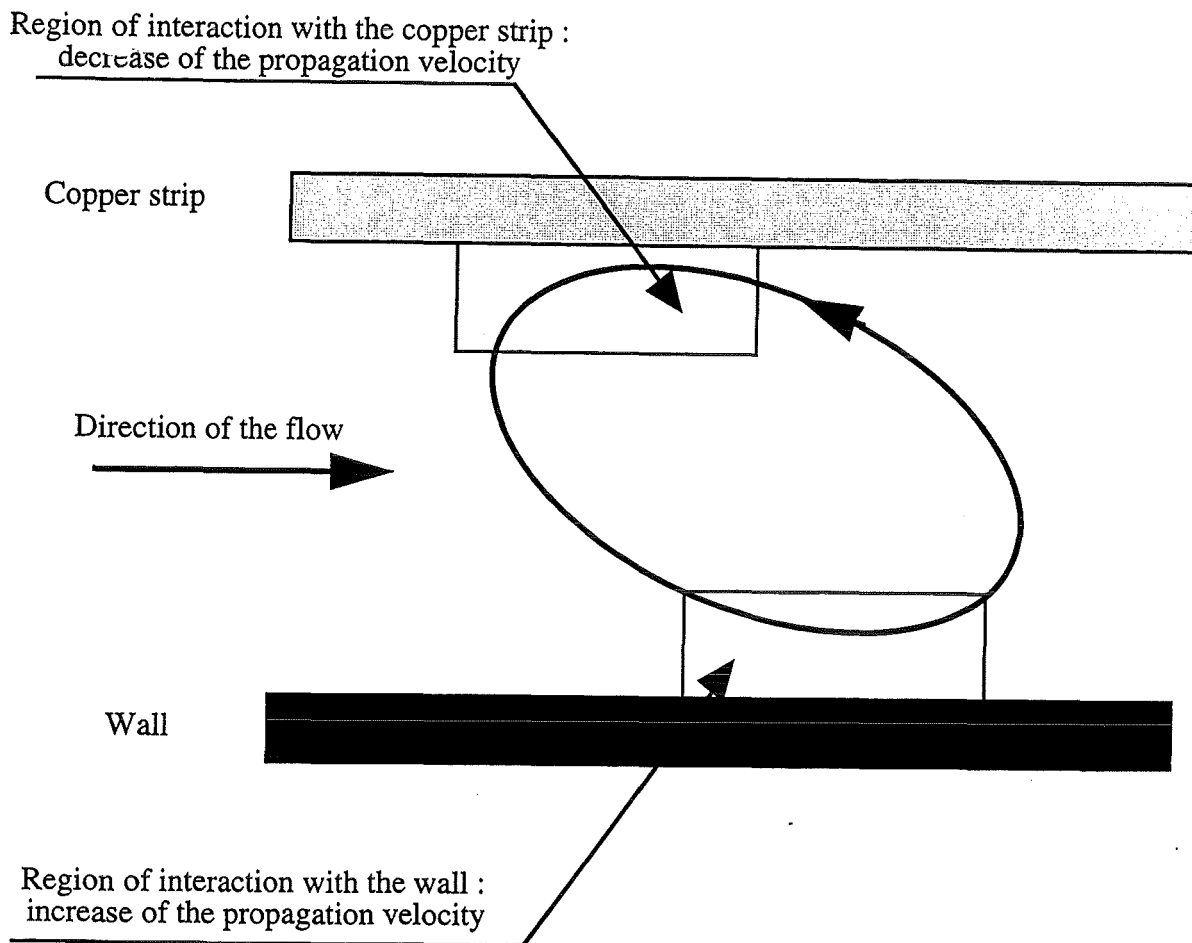


Fig. 15 : Principle of a vortex elongation due to interactions with the bounded experimental domain.

II-3.2 Power spectra

As we have seen before, time series measurements at one particular point or the correlation between two signals taken at different locations are the basic tools used to get the results previously displayed. As far as the search for the wavelength is concerned, an additional assumption is needed : the so-called Taylor's hypothesis. We will consider in this chapter some examples of time series measurements in order to explain what the main results are but also what their limitations are. The first series of measurements was performed in a relatively uniform manner as far as the acquisition rate and the data amount are concerned. However they do not always meet the ideal requirements for the purpose of comparison with the numerical results. This will logically lead later to conclusions in this report about what measurements should be performed in the future in order to get a better understanding of MHD instabilities and particularly a better insight into the link between the turbulence they generate and the increase of heat transfer that is initiated.

II.3.2.1 Comparisons between experimental and numerical results

Most of our measurements were performed with the same sampling frequency and the same number of acquired data : $(f_{\text{acq}}, N_{\text{data}}) = (330, 8192 = 2^{13})$. The main reason for the choice of this pair of acquisition parameters is the following. As already mentioned, these measurements were performed without any filtering. Hence we have to take into account the parasitic peaks which are coming from the power supply of the magnet. The dominant peak was observed to be located at 150 Hz. Therefore when choosing 330 Hz as the acquisition frequency, we avoid aliasing effects which could come from this peak. As far as the amount of data is concerned, for most of the measurements we stay with 8192 data per channel. It has to be recalled that for each pair of parameters (Re, M) we studied, a quasi-simultaneous measurement on ten channels was performed. Therefore each experimental file has an amount of 81920 data. From a technical point of view, the problem is not really the storage capacity but rather the access time to the hard disc which is becoming too long, diminishing the efficiency of the data treatment.

When performing FFT on the data file, the amount of data per channel 8192 is a necessary minimum to get a satisfactory precision for the final power spectrum. The Df resolution for a given data file is given by :

$$\Delta f = (f_{\text{acq}} / N_{\text{data}}) * C_{\text{window}}$$

with : f_{acq} : the acquisition frequency
 N_{data} : number of data,
 C_{window} : a coefficient > 1 depending on the window used.

For the purpose of windowing we used a Blackman-Harris window. This window is suitable for investigating steep spectra with minimum perturbation of the sample edges [6]. The C_{window} coefficient is then equal to 2. Despite the use of a window the spectrum will display some spurious non physical peaks when one does not perform an averaging operation. This averaging operation will be especially required when searching for inertial range in the power spectrum as we will see later on.

An averaging operation will consist of:

- * dividing the file in n equal pieces of data,
- * multiplying each of them by the Blackman-Harris window,
- * taking the square of the FFT of each pieces,
- * taking the average value of these squared FFT.

We also take the opportunity of making an overlapping between the successive sequences of data. This helps to increase the number of averaging sequences without increasing (in an arithmetic meaning) the frequency resolution f . In our case each sample overlaps the previous one by 25, 50, or 75%. Again we advise the reading of [7] to have a precise view on problems related to windowing and averaging on FFT.

The choice of the number n of equal sequences of data depends on the aim of the measurement. For the purpose of comparison with the computational results from the quasi 2D-model, taking into account the restricted available amount of data per channel, the number n of sequences of data to average should not be too large in order to avoid a lack of precision coming from a too large resolution in frequency. This problem can be understood through **Fig. 16 and 17**. They give the numerical and the experimental power spectrum respectively for the same pair of parameters $(Re, M) = (500, 566)$. As far as the numerical results are concerned the data file available is characterised by the pair $(f_{acq.}, N_{data}) = (111.2 \text{ Hz}, 6144 \text{ data})$. In order to get a readable spectrum we perform an averaging with 9 pieces of 2048 data. The overlapping is 75 %. Taking into account the fact that we used a Blackmann Harris window, this gives for the spectrum shown in **Fig. 20**, a frequency resolution of the order

$$\Delta f = 0.11 \text{ Hz.}$$

To be able to compare the computational with the experimental results we have to work with a roughly equal Df for the experimental power spectrum. As already mentioned before the experimental data file is characterised by the pair $(f_{acq.}, N_{data}) = (330 \text{ Hz}, 8192 \text{ data})$. Then performing an averaging with 5 sequences of data and an overlapping of 75 % gives

$$\Delta f = 0.16 \text{ Hz.}$$

As we can see from **Fig. 16 and 17** these Df are small enough to permit the comparison of the values of the largest peak in the two cases. But in fact, for the pair of parameters (Re, M) we display here $(500, 566)$, the behaviour of the flow is already strongly non linear. This means that both spectra exhibit in fact more than just one characteristic peak. Most are here hidden by a broadband spectrum because of the lack of resolution. In order to get a more precise comparison between the numerical and the experimental approach a smaller Δf is needed. From an experimental point of view we can afford this by means of a larger amount of data or lower data acquisition frequency. This last opportunity can only be achieved when filtering the signal in order to avoid perturbing aliasing phenomena.

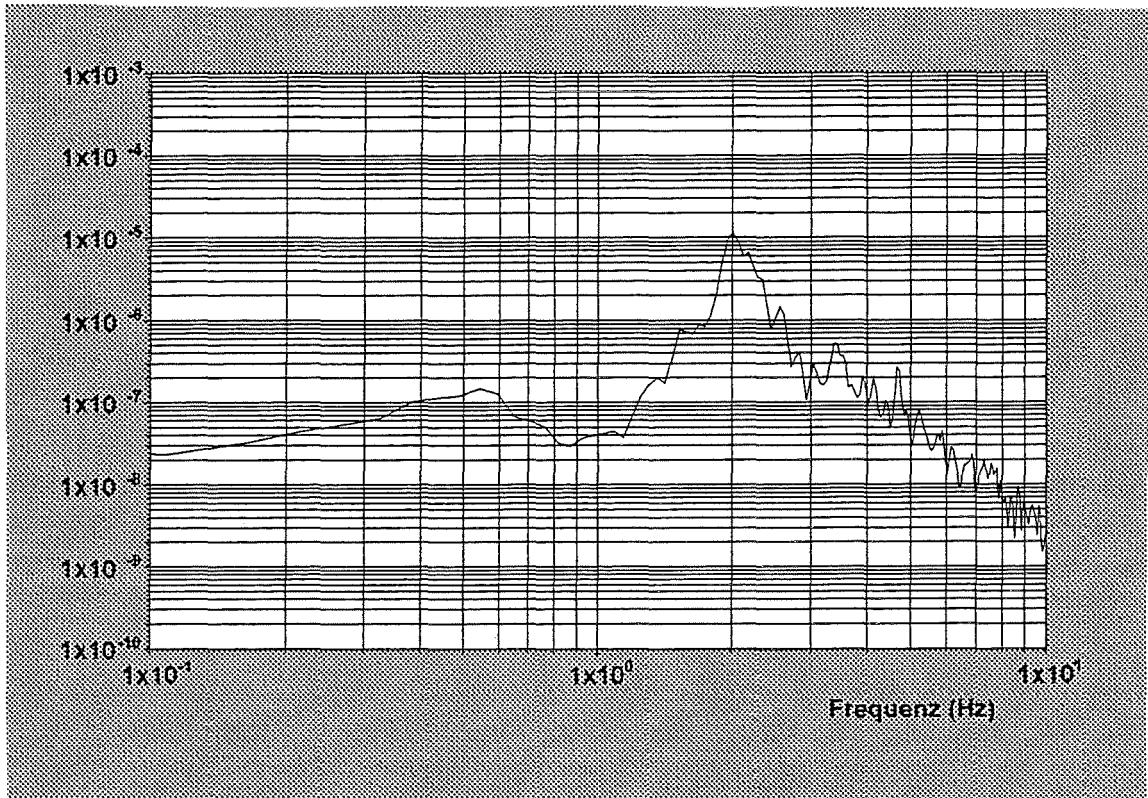


Fig. 16: Power spectrum as calculated from the numerical results for the pair of parameters $(Re, M) = (500, 566)$.

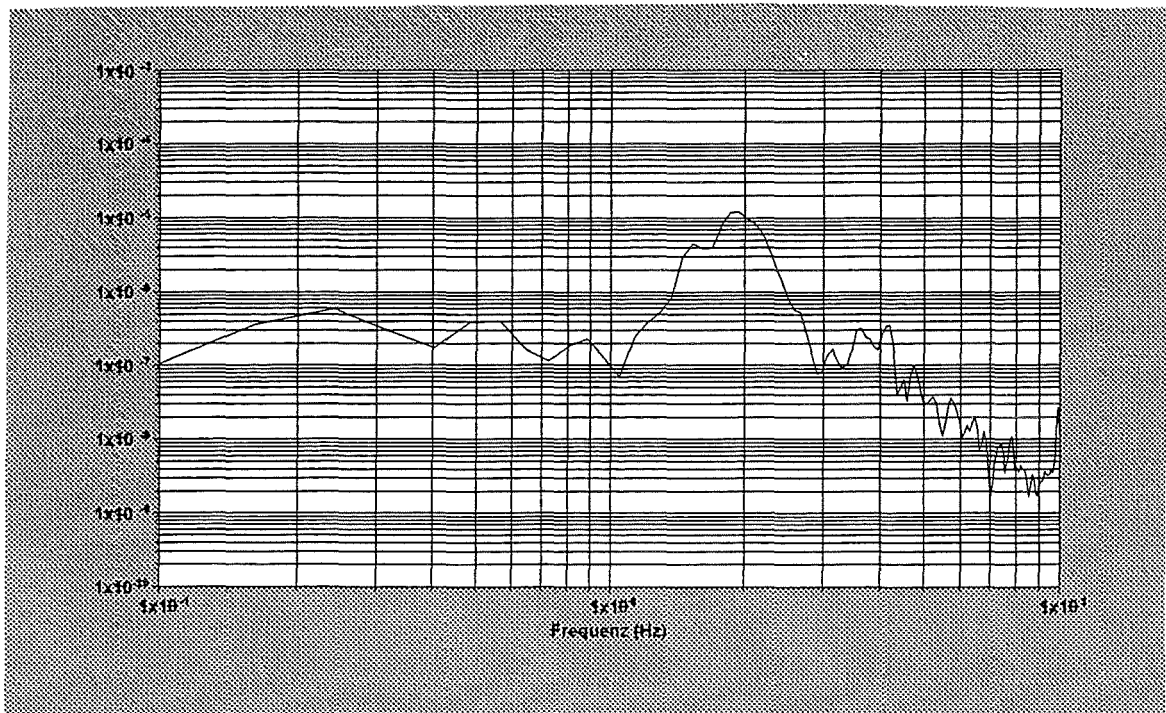


Fig. 17 : Power spectrum as calculated from the experimental results for the pair of parameters $(Re, M) = (500, 566)$.

II-3.2.2 Power spectra and turbulent behaviour

We now focus on spectra obtained for higher values of the Reynolds number. In this case, the flow is expected to show turbulent features. In the case of an isotropic homogeneous 2D turbulence forced at a given wave number (k_j). Kraichnan [8], taking into account the ideas developed by Kolmogorov for three dimensional turbulence, shows that the spatial power spectrum is characterised well by a double inertia range. One corresponds to an energy cascade from the wave number k_j to higher wavenumbers. The other is associated to an inverse energy cascade from the wave number k_j to lower wavenumbers. The proof of the existence of these inertia ranges has always been a big challenge from an experimental point of view, because precise measurements are required over, at least, one decade for the wavelength magnitude (see also the conclusion for this purpose).

We have to stress that in our case we are no longer dealing with the idealised case of 2D-homogeneous and isotropic turbulence, since in our experiments the flow is strongly confined by the lateral walls. Nevertheless, we believe that the spectral analysis can be a useful approach to get a better understanding of the physics related to this confined flow. Therefore we present now, by means of an example, the particular cases which have been taken in order to obtain correct power spectra.

3.2.2.1 Spectra compensation taking into account the spacing between the potential probes

This point is essential in order to retrieve valuable information from power spectra. The need for the compensation of the spectrum can be explained as follows. From an experimental point of view we are not measuring a local velocity but rather a mean velocity between two electrodes. And this has a big influence on the resulting spectrum. See for example [9].

Hence the measured velocity $V_{\text{meas.}}$ is given as a function of the true physical velocity V_{true} by :

$$V_{\text{meas.}}(x) = -\frac{1}{B} \frac{\Delta\phi}{\Delta X} = -\frac{1}{\Delta X} \int_{x_1}^{x_2} V_{\text{true}}(x) dx$$

Introducing the rectangular window, $P(a)$:

$P(\alpha) = 0$ when $|\alpha| > X/2$,
and $P(\alpha) = 1$ when $|\alpha| < X/2$,
we then have :

$$V_{\text{meas.}}(x) = \frac{1}{\Delta X} \int_{x_1}^{x_2} P(\alpha) V_{\text{true}}(x - \alpha) d\alpha$$

Taking the Fourier transform of the two terms of this equality we get:

$$\hat{V}_{\text{meas.}} = \frac{1}{\Delta X} \hat{P}(k) \hat{V}_{\text{true}}(k)$$

where k is the wave number and :

$$\hat{P}(k) = \Delta X \frac{\sin\left(\frac{k\Delta X}{2}\right)}{\frac{k\Delta X}{2}}$$

We have then finally the following relation between the real power spectrum $E_{\text{true}}(k)$ and the measured power spectrum $E_{\text{meas.}}(k)$:

$$E_{\text{true}} = \frac{E_{\text{meas.}}(k)}{\left(\sin\left(\frac{k\Delta X}{2}\right)\right)^2} \left(\frac{k\Delta X}{2}\right)^2$$

Unfortunately there is a lack of precision in numerous papers that prevents the reader from knowing whether this correction had been performed or not. As we will see later on this can have a strong effect on the slopes observed in the power spectra.

3.2.2.2 The Taylor's hypothesis

To get a spatial power spectrum in terms of k , the most direct way is to use a line of potential electrodes regularly spaced. This will provide a one dimensional power spectrum in the sense that it is calculated with only one component of the velocity in the plane. It can be shown that when the power spectrum exhibits a power law, the one dimensional spectrum will exhibit the same one. (See for example [5] for a summary of this kind of notation). In the case of the first series of measurements we use the 23 probe array together with a bank of 10 amplifiers on one card. The wiring was such that only 4 quasi-simultaneous measurements were performed on a line. Therefore it would have been nonsense to search for a spatial power spectrum with so small a number of measurements. (This would no longer be the case with the new probe array that will allow 11 individual measurements on a streamwise line.) Accordingly the spectra we get were obtained using a one point time series measurement and assuming, in the first order, the validity of the Taylor's hypothesis. This latter means that when the velocity fluctuations of a given flow are small as compared to the mean velocity of the flow V_{mean} , one can correlate the time fluctuations $u(t)$ to the spatial fluctuations $u(x/V_{\text{mean}})$. This means that a wave number can be associated to a characteristic frequency given by a local time measurement in the flow. The relation is given by:

$$k = \frac{2\pi}{\lambda} = \frac{2\pi f}{V_{\text{mean}}}$$

Then, if the validity of the Taylor's hypothesis is assumed, the time power spectrum will exhibit the same slope as the corresponding spatial spectrum. The compensation of the spectrum due to the finite potential probe spacing can also be taken into account in the temporal domain spectra. Next we display an example of temporal power spectrum **Fig. 18** for the following pair of parameters : $(Re, M) = (3000, 300)$. The figure displays both the original and the compensated power spectrum. The difference between the two spectra at higher frequencies shows clearly the error that can be made, when one does not take into account the finite spacing between the potential probes.

In order to obtain this smooth spectrum, the data file we used was characterised by the following pair of acquisition parameters : $(f_{acq}, N_{data}) = (220 \text{ Hz}, 32768 = 2^{15} \text{ data})$. We then perform an averaging of 253 sequences of 512 data with an overlapping of 75 %. The Δf resolution is then about 0.84 Hz.

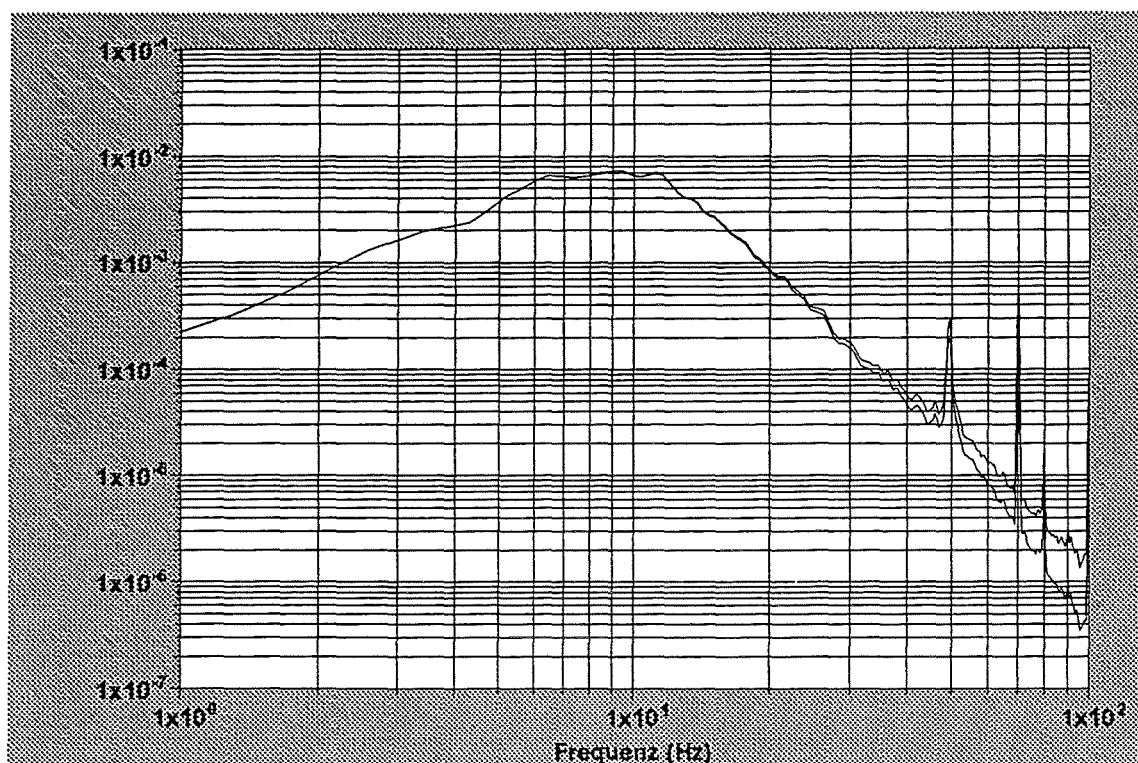


Fig 18 : Power spectrum as calculated from the experimental results for the pair of parameters $(Re, M) = (3000, 300)$. The upper line corresponds to the compensated spectrum, the other one to the original. The origin of the peak at 50 Hz is clear. The peak at 70 Hz and at 80 Hz are due to aliasing phenomena coming from the lower acquisition frequency used in this case. (220 instead of 330 Hz).

As can be seen on **Fig. 18** a mean slope can be extracted from the log-log representation of the spectrum. This slope is approximately -3.5. The main conclusion is that we were able to observe an inertial behaviour over a frequency decade (correspondingly over a wavelength decade when assuming Taylor's hypothesis). Hence the dominant frequency in this spectrum is about 10 Hz. This corresponds to the frequency at which the energy is injected by means of the instability occurring due to the copper strip in the middle of Hartmann wall of the channel. This frequency corresponds to a non dimensional wavelength of 17 as can be seen from **Fig. 11** which displays the variation of the wavelength with the Reynolds number for the value of $M=300$ we have considered here. The maximum frequency of 100 Hz which is displayed here corresponds to a wavelength of 1.7. This value is still significantly larger than the probe spacing giving the normalisation of the wavelength.

No inverse cascade is observed. This is quite logical if one considers the following argument. As we have seen from **Fig. 12** which displays an example of the results obtained by a numerical approach, the wavelength increases clearly in the direction of the flow. This agrees well with the basic tendency of 2D flows to generate larger and larger structures. But as we have concluded from the study of the changes of the wavelength with an increasing Reynolds number, the presence of lateral channel walls inhibits the unlimited growth of the wavelength. For the pair of parameter $(Re, M) = (3000, 300)$ we consider here, the mean wavelength has already reached the maximum size. It can then be concluded that the injection of energy is made at this maximum scale depending on the channel width. Therefore the mechanism of inverse cascade does not apply due to the presence of the lateral walls.

At this stage, it is difficult to extract more from this temporal power spectrum for at least the two following reasons.

First, there is still the lack of theoretical results associated with this kind of strongly confined turbulent MHD flow. The main feature that is actually not taken into account in the quasi 2D numerical model is the strong interaction that might occur between the vortical structures and the outer wall. Hence, as we have seen before, for high Reynolds numbers, the vortices initiated by the primary shear are reaching the lateral walls and certainly start to interact. This has already been shown by a 3D numerical model developed by L. Leboucher [10] who performed some calculations for comparison with our experimental data. These computations show that even for moderate Reynolds numbers, an interaction between the primary vortex and the side layers can occur. Hence, it is numerically observed that once the primary vortex had reached the outer wall, the interaction with the side layer initiates secondary vortices which can even become predominant in the flow. The complexity of these events shows the need for obtaining a vorticity distribution image from the experiments in order to compare these images directly with the numerical predictions. By now, the two-line measurements we performed permit a check on the validity of the linear analysis and also of some non linear features. Our measurements have been performed particularly close to the central copper strip. However

following the transverse direction from the copper to the outer wall, the dominant physical phenomena of the flow seem to change drastically.

We hope that the use of the new 6*11 probe array will help to provide a better understanding of these yet unidentified phenomena.

Secondly there is a limitation due to the use of Taylor's hypothesis. In fact, in our case its use is quite difficult to justify. Following R. Leboeuf and R. Mehta [11], the four main causes for the breakdown of Taylor hypothesis have been identified as :

- temporal evolution of the flow field,
- non uniformity of propagation velocity,
- anisotropy produced by the primary shear,
- aliasing due to an unsteadiness in propagation velocity.

It is then difficult to justify the application of the Taylor's hypothesis for our case. Firstly there is a flow anisotropy induced by the primary shear in our case; and secondly the non uniformity of the propagation velocity might be important. Therefore, as we have just realised, at least above a critical Reynolds number, the primary shear due to the copper strip, induces vortices whose size is of the order of the channel width. If the vorticity of these structures is high enough, they can induce a kind of secondary flow. The latter will then lower the flow velocity in the region near the copper strip edges and accelerate it near the outer wall. Then the smaller vortices, if they exist, will be convected by the modified flow. The basic mechanism is sketched in **Fig. 19**. We see that it finally leads to different propagation velocities depending on the size and on the location of the considered flow structure.

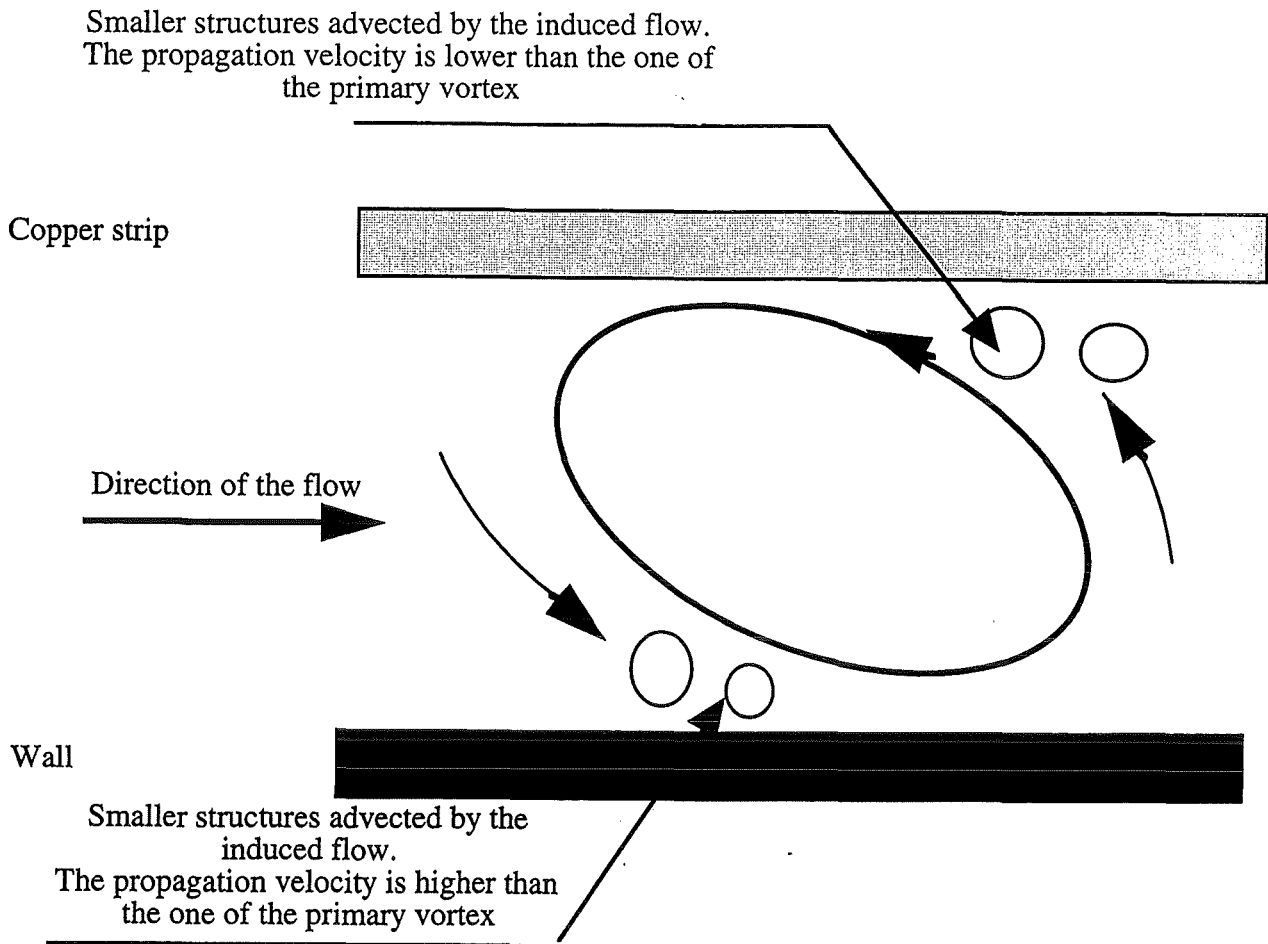


Fig. 19 : Sketch showing the influence of the main vortex on the propagation velocity of the smaller structures.

We can try to understand what is the main consequence of the change of the propagation velocity on the slope of the temporal power spectrum. Two cases are then to be considered depending on the transverse location of the probe.

First, the probe is located near the copper strip (this is the case of the measurement displayed in **Fig. 18**). As we have just explained, the propagation velocity would then be lower for the smaller structure. When applying Taylor's hypothesis, which associates to a given frequency a defined wave number by means of a linear relationship, this implies that we underestimate the values of k associated with the higher frequencies of the spectrum. Then we think that a spatial power spectrum obtained with a measurement along a line located near the copper strip in the streamwise direction will display a lower slope for the inertia range than the one found for the temporal power spectrum.

Secondly, the probe is located near the outer wall. The velocity of the smaller structures would then become higher than the mean propagation velocity of the larger vortices. We then obtain the reverse result from the previous case. A spatial power spectrum obtained with a measurement along a line located near the outer wall in the streamwise direction will display a larger slope for the inertia range than the one found for the temporal power spectrum.

III-BEFORE CONCLUDING : A GLIMPSE AT 2D TURBULENCE RESEARCH

Many investigations are now being performed to get a better insight into the dynamics of vortices in 2D-flows. This is motivated by the number of scientific fields concerned with this particular field of fluid dynamics, e.g. meteorology, oceanography, fusion or metallurgical applications working with strong magnetic fields.

The classical approach of 2D-turbulent flows was developed by Kraichnan, taking into account a theory derived some years before by Kolmogorov for 3D-turbulent flows. In both cases, the underlying idea is to consider that the flow forced by the inertia dominating effects behaves in a self-similar manner within a certain spatial scale range. It means that no preferential scales are detected in the flow except for the scales associated with the limits of the inertia range. The characteristic of this inertia range concept in the energy spectrum of the flow must be simple power laws for the energy decrease with increasing wavenumbers.

Consequently, for at least two decades, the experimental challenge in this field was to check this nice elegant theory. Unfortunately, it was not so easy to perform.

The main problem is in fact the finite range of observable scales. This range is always bounded from above by the maximum size of the experimental facility and bounded at the lower side by measurement limitations which in fact come mostly before the viscous scale becomes important.

A second point is a more philosophical one. It consists in claiming that the connection between a given theory and experimental results is not only a matter of basic comparison. For instance a model, with its simplicity and its mathematical efficiency can be so attractive that finally it could distract us from the reality... if there is any. Quantum mechanics has already made us understand that the reality depends on the observer from an experimental point of view. Without involving any quantitative point of view, we can nevertheless additionally say that the observer influences the reality by the subjective view he has adopted with a given theory. Be careful! It does not mean that he is cheating by the experimental results, (it happens however sometimes!). It only means that, the physical reality can be seen through different filters brought by the observer himself. Hence, the observer, however open-minded he may be, cannot observe any physical phenomenon without having a preoccupation of interpretation. This preoccupation could either originate from a given theory, or from his own personal intuition. This last case is not yet our purpose, so we will lay it aside. The problem occurs when the filters become so strong, that they inhibit the emergence of new ideas. It is then useful to change ones point of view to

make a new step towards the insight of the physics of a given phenomenon (stated that the principal mission of a physicist is to question and not to live comfortably with a peaceful well-established theory).

In the case of 2D-turbulence, this change in the point of view happened roughly ten years ago. It is the consequence of the answer given by the scientific community to the following question : Are you really sure that there is no preferential scale in the flow? It is quite impossible to say exactly who was the first to raise this question. Nevertheless, the weight of this very practical point of view was not negligible in the balance. Hence we can roughly identify the following process.

First step. New theoretical ideas were raised in the scientific community about turbulence (2D or 3D, no matter for the present purpose).

Second step. These ideas penetrated the domain of applied sciences where the description of turbulence was urgently required, e.g. meteorology, aeronautics. Researchers in this field after having taken into account these new concepts raised practical questions such as :

- How can a typhoon be described by your theory ?
- The biggest problem in turbulent flow is the detachment of vortices the wing tips of the plane. I don't see any vortices in your theory !

The reaction of the scientists can be summarised as follows. They claim that they have also observed this kind of phenomena, but argue that these are always linked to end effects. The turbulence theory is only valid in the case of an homogenous isotropic turbulence which *takes place*...in an unbounded domain. As the notion of turbulence is at 90 % related to the field of the fluid mechanics, one of the branches of the physics most closely related to technical applications, they had, for obvious reasons if not compulsorily, to change the orientation of their research relatively quickly.

Scientists tried to take into account the influence of bounded domains which introduces in fact a characteristic size depending on each experimental set-up. But as we are interested in highly non-linear phenomena, this characteristic length scale cannot be simply considered as the particular length scale which bounds the application of the theory of Kraichnan. In fact interactions of the flow with the physical boundary can be so strong that they could govern the whole flow. This fact contributes to the development of a new approach on turbulent flows which pays more attention to the structure of the flow itself. This new impulse has led to the idea (in the field of 2D-flows), of starting a new view for the turbulence taking into account the fact that for each "blind" wavelength in an energy spectrum there exists in reality a physical structure of finite size. Then, even for almost total inertial flows, the specialists are now used to talking about "the dynamics of vortices" when dealing with 2D-turbulent flows. This is not only a matter of wording but has a great influence on the way the experiments are designed.

The GALINKA and MATUR experiments in Karlsruhe and Grenoble are two good examples of the actual orientation which is given to the research on 2D-turbulent flows. Their characteristic sizes are not large, as the effects of the boundary on the flow are not intended to be neglected. On the contrary, one of the final aims of those experiments is to

integrate the influence of the walls into the analytical models. The potential probes developed in both cases are similar and they are located so that the information they give enable us to build an image of the flow structure.

This experimental study of the 2D-dynamics of vortices in the presence of boundaries is essential for the purpose of applications where the flows are always bounded. From a theoretical point of view, it can be seen, at a first glance, as the revenge of an old school of physicists which would have never deeply integrated the statistical approach of turbulence and would have tried desperately to deal with a more *mechanistic* approach which could allow, once more, deterministic reasoning to be efficient. At a second glance, one can see that statistical tools and related manners of thinking, are already well cast in the brains of most of the physicists. Then new statistical approaches are developed for 2D-flow dynamics, which benefit from the knowledge accumulated in statistical thermodynamics. This is specific to 2D-flows, thanks to the existence of conservative quantities where the vorticity is then the unavoidable most important physical quantity. This new approach will be of great benefit for the study of fluid mechanics, without prejudging the results to come, in the sense that it forces scientists from different branches to work together. This is not easy because we deal here with almost the worst case as fluid mechanicians and physicists have to work together.

Then, the new generation of experimental facilities as GALINKA at IATF or MATUR at the EPM-MADYLAM laboratory encounters a great challenge, as they must be able to serve as a guide for new analytical models and simultaneously to answer some more technical questions linked to peculiar applications.

This is the key point, and both IATF and EPM-MADYLAM laboratory are well placed for this challenge, since applied and theoretical investigations are performed *on the same experimental facility*.

IV-CONCLUSIONS

The GALINKA facility was constructed as closely as possible to the "theoretical configuration" used by L. Bühler for his computations on the influence of inhomogeneous conductivity of the Hartmann wall in a ducted flow. This allows us to obtain detailed comparisons between what can be called the numerical approach and the experimental performance, as we have shown on previous pages.

From a technical point of view, the potential probe arrays have been carefully prepared so that the experimental results obtained are the most precise ones performed in the field of velocity characterisation of 2D-MHD flows. This is due to the knowledge which the team at IATF in Karlsruhe had acquired concerning the use of the In/Ga/Sn alloys in past years. When using mercury for instance, the behaviour of this metal, regarding amalgamation processes, leads to the use of larger potential probe diameters to avoid electrical contact problems. The resolution of the velocity field is then reduced. It is also noteworthy that the GALINKA facility has a removable test section which can be easily replaced for the purpose of other research objectives. Moreover, the potential probe arrays can be inserted in any new test section.

But one can say that an experiment has been successful when the precision of the measurements performed are suitable not only to check previous analytical predictions, but also to point out new physical features. I think that we have started to succeed in this direction. Indeed, we have shown in this report that the measurements we get in the non linear regime, far away from the stability threshold of the flows, exhibit some strange features which can hardly be taken into account by a 2D-approach neglecting the influence of the lateral walls. In some cases the experimental results should be seen as a guide in order to develop new models or to check 3D-calculations that are now being used at the IATF.

For further comparisons with the numerical predictions, one should be able to retrieve from the measurements a chart of the velocity and vorticity field. For this purpose we need the use of the new probe array we developed. The next step will then be to obtain a direct image of the flow by this new observation tool as the main technical problems seem to be solved. This will allow us to get a better understanding of the flow especially concerning the expected interactions with the lateral walls. From our point of view, this task should be considered as a priority, both, for practical applications (where unbounded domains are seldom encountered!) and for the sake of comparisons with theoretical approaches. As already known in the purely hydrodynamic case [6], the non linear interactions of vortices with lateral walls might lead to complex channel flow patterns. Then the direct experimental visualisation of these interactions is needed in the case of flows under magnetic fields to achieve the development of an underlying theory.

To summarise, we think that a valuable step in the understanding of these phenomena might only be achieved under the condition of a close interaction between theorists and experimentalists. I hope that we have already achieved a significant step in this direction.

V-REFERENCES

- [1] L. Barleon, K. J. Mack, R. Stieglitz, (1996) : *The MEKKA-facility a Flexible Tool to Investigate MHD-flow Phenomena*. Wissenschaftliche Berichte, FZKA report 5821.
- [2] Yu B. Kolesnikov (1972) : *Two dimensional turbulent flow in a channel with inhomogeneous electrical conductivity of the wall*. Magnetohydrodynamics **3**, 308-312.
- [3] L. Bühler (1994) : *Instabilities in 2D MHD flows*.
Proceeding of the 2nd International Conf. on Energy Transfer in MHD Flows, PAMIR, Aussois, France, Sept. 26-30, 1994, **2** 463-472
- [4] L. Bühler (1995) : *Instabilities in quasi two dimensional magnetohydrodynamic flows*.
Journal of Fluid Mechanics, **326** 125-50.
- [5] J. Sommeria (1986) : *Experimental study of the two-dimensional inverse energy cascade in a square box*. Journal of Fluid Mechanics, **170** 139-168.
- [6] T. L. Doligalski, C. R. Smith, J. D. A. Walker (1994) : *Vortex interaction with walls*
Annu. Rev. Fluid. Mech., **26** 573-613.
- [7] F.J. Harris (1978) : *On the use of windows for harmonic analysis with the discrete Fourier transform*. Proc. IEEE **66** (1) 51-83.
- [8] R. H. Kraichnan (1967) : *Inertial ranges in two-dimensional flow*.
Phys. Fluids **10** 1417.
- [9] J. M. Nguyen Duc (1988) : *Instabilité et turbulence dans des écoulements bidimensionnels MHD*. Thèse INP Grenoble. France.
- [10] L. Leboucher (1995) : *Numerical simulations of unsteady MHD flows in ducts*.
Wissenschaftliche Berichte, FZKA report 5663.
- [11] R. L. LeBoeuf, R. D. Mehta (1995) : *On using Taylor's hypothesis for three dimensional mixing layers*. Phys. Fluid. **7**(6) 1516-1518.